HHS Public Access

Author manuscript

Nat Microbiol. Author manuscript; available in PMC 2018 March 04.

Published in final edited form as:

Nat Microbiol. 2017 November ; 2(11): 1543–1557. doi:10.1038/s41564-017-0017-2.

TRIM23 mediates virus-induced autophagy via activation of TBK1

Konstantin M.J. Sparrer[1,^], **Sebastian Gableske**[1,^], **Matthew A. Zurenski**[1], **Zachary M. Parker**[1], **Florian Full**[1], **Gavin J. Baumgart**[1], **Jiro Kato**[2], **Gustavo Pacheco-Rodriguez**[2], **Chengyu Liang**[3], **Owen Pornillos**[4], **Joel Moss**[2], **Martha Vaughan**[2], and **Michaela U. Gack**[1,*]

[1]Department of Microbiology, The University of Chicago, Chicago, Illinois 60637, USA

[2]Cardiovascular and Pulmonary Branch, National Heart, Lung, and Blood Institute, National Institutes of Health, Bethesda, Maryland 20892, USA

[3]Department of Molecular Microbiology and Immunology, Keck School of Medicine, University of Southern California, Los Angeles, California 90033, USA

[4]Department of Molecular Physiology and Biological Physics, University of Virginia, Charlottesville, Virginia 22908, USA

Abstract

Autophagy and interferon (IFN)-mediated innate immunity are critical antiviral defense mechanisms, and recent evidence indicated that *tripartite motif* (TRIM) proteins are important regulators of both processes. While the role of TRIM proteins in modulating antiviral cytokine responses has been well established, much less is known about their involvement in autophagy in response to different viral pathogens. Through a targeted RNAi screen examining the relevance of selected TRIM proteins in autophagy induced by herpes simplex virus 1 (HSV-1), encephalomyocarditis virus (EMCV), and influenza A virus (IAV), we identified several TRIM proteins that regulated autophagy in a virus-species specific manner, as well as a few TRIM proteins that were essential for autophagy triggered by all three viruses and rapamycin, among them TRIM23. TRIM23 was critical for autophagy-mediated restriction of multiple viruses, and this activity was dependent on both its RING E3 ligase and ADP-ribosylation factor (ARF) GTPase activity. Mechanistic studies revealed that unconventional K27-linked auto-ubiquitination of the ARF domain is essential for the GTP hydrolysis activity of TRIM23 and activation of TANK-binding kinase 1 (TBK1) by facilitating its dimerization and ability to phosphorylate the selective autophagy receptor p62. Our work identifies the TRIM23-TBK1-p62 axis as a key

*Correspondence should be addressed to M.U.G. (mgack@uchicago.edu).
^These authors contributed equally.

AUTHOR CONTRIBUTIONS

K.M.J.S., S.G., and M.U.G conceived and designed the experiments. K.M.J.S and S.G. performed and analyzed all experiments, except those in Supplementary Fig. 4f (M.A.Z.), Supplementary Fig. 2c (F.F), and Fig. 5e (Z.M.P). G.B. performed mutagenesis experiments. J.K., G.P.-R., J.M., and M.V. provided *TRIM23* $^{-/-}$ and WT MEFs. C.L. contributed reagents, materials and analysis tools for experiments. O.P. performed the TRIM23 ARF structure modeling. K.M.J.S. and M.U.G wrote the manuscript.

COMPETING FINANCIAL INTERESTS

The authors declare no competing financial interests.

component of selective autophagy and further reveals a role for K27-linked ubiquitination in GTPase-dependent TBK1 activation.

INTRODUCTION

TRIM proteins are key components of the innate immune system, functioning as antiviral restriction factors, or modulating signaling cascades that lead to proinflammatory cytokine induction[1,2]. Moreover, several TRIM proteins also regulate fundamental cellular processes such as cell proliferation and differentiation, gene transcription, and RNA metabolism. TRIM proteins belong to the larger family of RING E3 ligases and can synthesize both classical degradative K48-linked ubiquitination, and various non-degradative polyubiquitin-linkage types. For most TRIM proteins, RING E3 enzymatic activity is required for their ability to restrict viral infection or modulate innate immune signaling[1].

Autophagy is an evolutionarily conserved and highly regulated homeostatic process in which damaged or surplus proteins and organelles are engulfed by double-membrane structures called autophagosomes and subsequently degraded by the lysosome[3]. Although autophagy was initially described as a non-specific auto-digestive response towards nutrient depletion, it has become evident that autophagy also selectively recognizes and degrades ‘tagged’ cargos via autophagy receptors, such as p62/SQSTM1, Optineurin and NDP52[4]. Upon recognition via ubiquitin, galectin, or other ‘earmarks’, cargos are delivered by these receptors to microtubule-associated protein light chain 3 (LC3)-containing autophagosomes to induce cargo degradation[5].

Autophagy is implicated in diverse physiological functions in humans, including stress adaptation, development, and protection against inflammation and neurodegeneration[3]. Furthermore, autophagy has been increasingly appreciated as an important mechanism in antimicrobial defenses[6–8]. In regards to viral infection, it has been shown that autophagy can either promote or suppress viral replication, dependent on the viral pathogen, host species, and cell type. Recent studies demonstrated that autophagy and antiviral innate immune responses, in particular the type I interferon (IFN) response, are intricately interconnected[6,8], and several key molecules involved in innate immunity are also important regulators of autophagy. For example, TANK-binding kinase 1 (TBK1) phosphorylates IFN-regulatory factor 3 and p62 to induce IFN-β induction and autophagy, respectively[9–11]. NOD-like receptor family member X1 (NLRX1) suppresses RIG-I-mediated IFN-β gene expression, while promoting virus-induced autophagy[12,13]. Moreover, it has recently been demonstrated that TRIM proteins, which are well known to regulate antiviral cytokine responses, also play important roles in virus-induced autophagy and autophagy-mediated antiviral defenses[2,14]. For example, TRIM5α was shown to mediate autophagy-dependent degradation of the capsid of human immunodeficiency virus 1 (HIV-1)[14]. However, compared to the wealth of information about TRIM-mediated regulation of antiviral cytokine responses, our knowledge about the functional role of TRIM family members in autophagy in response to different viral pathogens is still rudimentary.

Here, we show that TRIM proteins play important roles in virus-triggered autophagy in a virus species-specific manner. We further identify TRIM23, which has dual E3 ubiquitin

ligase and GTPase activities, as a core component of the selective autophagic machinery. TRIM23 GTP hydrolysis activity is activated through K27-linked auto-polyubiquitination, which is essential for the recruitment of TRIM23 to autophagosomal membranes and activation of TBK1- and p62-mediated selective autophagy.

RESULTS

Virus-specific roles of TRIM proteins in autophagy

To systematically assess the role of TRIM proteins in autophagy, we first screened a cDNA library of 61 TRIM proteins for their ability to induce formation of green fluorescent protein (GFP)-LC3B puncta in human cells, which is a hallmark of autophagy induction (Fig. 1a,b and Supplementary Fig. 1a). 18 TRIM proteins efficiently induced GFP-LC3B puncta, to a greater extent than even treatment with the mTOR-inhibitory drug rapamycin, which robustly activates autophagy and thus served as a positive control. 31 TRIM proteins detectably induced GFP-LC3B puncta formation as compared to empty vector transfection, although less efficiently than rapamycin (Fig. 1a,b and Supplementary Fig. 1a). The seven TRIM proteins (TRIM 23, 25, 38, 41, 44, 61 and 74) that most strongly induced GFP-LC3B puncta formation also effectively induced processing of endogenous LC3B-I to LC3B-II (Supplementary Fig. 1b).

As many viral pathogens induce autophagic flux in infected host cells, we next asked whether the TRIM proteins identified by our cDNA screen are essential for virus-induced autophagy. To this end, we determined the effect of small interfering RNA (siRNA)-mediated knockdown of selected TRIM proteins on GFP-LC3B puncta formation in response to infection by three different viral pathogens known to induce autophagy: *1)* influenza A virus (IAV), a negative-strand RNA virus of the *Orthomyxoviridae* family; *2)* encephalomyocarditis virus (EMCV), which is a *Picornaviridae* family member carrying a positive-strand RNA genome; and *3)* a mutant variant of herpes simplex virus 1 (a dsDNA virus), in which the Beclin-1-binding domain[15] of the autophagy-antagonistic protein γ34.5/ICP34.5 is deleted[16] (hereafter referred to as mutHSV-1) (Fig. 1c–f and Supplementary Fig. 1c). In parallel, we also determined the effect of depleting individual TRIM genes on GFP-LC3B puncta formation induced by rapamycin (Supplementary Fig. 1d). Non-targeting scrambled siRNA (NT) and siRNAs targeting the autophagy-related genes 5, 7 or 12 (ATG 5, 7, or 12), which are core components of the cellular autophagy machinery, served as controls. The knockdown efficiency of the individual TRIM proteins was determined by qPCR (Supplementary Fig. 1e), and efficient viral infection in our screen was confirmed by immunofluorescence staining of specific viral proteins (Supplementary Fig. 1f). Depletion of several TRIM proteins significantly reduced GFP-LC3B puncta induced by a specific virus (*e.g.* TRIM13 for EMCV; TRIM25 for IAV; and TRIM56 for mutHSV-1) (Fig. 1c–f). Knockdown of other TRIM proteins (*e.g.* TRIM20, TRIM38, TRIM44, and TRIM74) abrogated autophagy induced by infection with a specific virus and also rapamycin (Fig. 1c–f), suggesting overlap between the autophagy initiation pathways triggered by viral infection and mTOR inhibition. Finally, silencing of endogenous TRIM21, TRIM23, and TRIM41 profoundly decreased autophagy induced by all three viruses as well as rapamycin, to a

similar extent as knockdown of ATG5, ATG7 or ATG12, suggesting that these TRIM proteins play a central role in the autophagic process.

TRIM23 is essential for autophagy in response to viral infection

Both our cDNA and RNAi screens suggested that TRIM23 is an important molecule in autophagy, which is a fundamental process in vertebrates, invertebrates, and yeast. Sequence alignment showed that TRIM23 is highly conserved in vertebrates and also *C. elegans* (Supplementary Fig. 2a); however, no orthologous TRIM23 sequence was identified in yeast. TRIM23 transcripts were readily detectable in many different human tissues (Supplementary Fig. 2b). Furthermore, in contrast to many TRIM proteins which are expressed at low levels under normal conditions and are inducible by type I IFN[1], TRIM23 mRNA was not upregulated upon IFN-α stimulation or infection with Sendai virus (SeV), which is known to robustly induce type I IFNs (Supplementary Fig. 2c). In line with this, endogenous TRIM23 protein was readily detectable under normal (unstimulated) conditions, and its abundance did not change upon IFN-α stimulation or SeV infection (Supplementary Fig. 2d).

To corroborate the role of TRIM23 in autophagy, we first compared the effect of ectopically expressed FLAG-TRIM23 on GFP-LC3B puncta formation and conversion of endogenous LC3B-I to LC3B-II in wild-type (WT) mouse embryonic fibroblasts (MEFs) and MEFs that are deficient in *ATG5* (*ATG5* $^{-/-}$ MEFs)[17]. FLAG-TRIM23 efficiently induced LC3B puncta formation and LC3B-I/II processing in WT MEFs, but not *ATG5* $^{-/-}$ MEFs. (Supplementary Fig. 3a–c). To confirm the data from our siRNA screen, we silenced endogenous TRIM23 using a small hairpin RNA (shRNA) that has a different TRIM23-targeting sequence than the siRNAs used. ShRNA-mediated knockdown of TRIM23 profoundly reduced the number of GFP-LC3B puncta that formed upon infection with mutHSV-1, IAV, or respiratory syncytial virus (RSV) of the family *Paramyxoviridae* (Supplementary Fig. 3d–f). Consistent with the results from our siRNA screen, shRNA-mediated TRIM23 depletion also markedly reduced GFP-LC3B puncta formation and LC3B-I/II conversion induced by rapamycin (Supplementary Fig. 3g–i). We next utilized MEFs from *TRIM23* $^{-/-}$ and WT mice[18] to confirm the role of TRIM23 in autophagy. While mutHSV-1 infection and rapamycin treatment efficiently induced LC3B puncta formation in WT MEFs, the numbers of LC3B puncta were very low in infected *TRIM23* $^{-/-}$ MEFs, similar to those in untreated (Mock) cells (Fig. 2a–c). In line with this, endogenous LC3B puncta accumulated in rapamycin-treated or mutHSV-1-infected WT, but not *TRIM23* $^{-/-}$, cells (Supplementary Fig. 4a). TRIM23 gene targeting also abrogated LC3B puncta formation induced by infection with a GFP-expressing recombinant human adenovirus (Ad-GFP, a dsDNA virus) or Sindbis virus (SINV, an alphavirus with a positive-strand RNA genome), further strengthening that TRIM23 is important for autophagy triggered by a broad range of viruses (Fig. 2d,e **and** Supplementary Fig. 4b,c). Notably, gene targeting of TRIM23 had only a minor or no effect on basal or starvation-induced autophagy, respectively (Fig. 2a–e and Supplementary Fig. 4d,e).

Another hallmark of autophagic flux is the degradation of the selective autophagy receptor p62[19,20]. Whereas endogenous p62 was degraded in WT MEFs in response to mutHSV-1

infection or rapamycin treatment, it was stabilized and abundant in *TRIM23* $^{-/-}$ MEFs (Fig. 2f). However, the increased protein abundance of p62 in *TRIM23*$^{-/-}$ MEFs was not due to transcriptional upregulation of p62 in these cells (Supplementary Fig. 4f). Electron microscopy (EM) confirmed that WT, but not *TRIM23*$^{-/-}$, MEFs contained a large number of autophagolysosomes following mutHSV-1 infection or stimulation by rapamycin (Fig. 2g).

EM analysis also showed that mutHSV-1-infected *TRIM23* $^{-/-}$ MEFs had an increased number of virus particles in the cytoplasm as compared to infected WT cells (Fig. 2g), suggesting that TRIM23-mediated autophagy acts in an antiviral manner. To test this directly, we analyzed HSV-1 replication in WT and *TRIM23* $^{-/-}$ MEFs (Fig. 2h). As TRIM23 reportedly also plays a role in type I IFN responses[21,22], we sought to compare the growth of WT HSV-1 and mutHSV-1, the latter lacking a major autophagy-antagonistic mechanism due to mutation in the γ34.5 protein[15], and therefore efficiently inducing LC3B-I/II conversion in contrast to WT HSV-1 (Supplementary Fig. 4g). However, both WT HSV-1 and mutHSV-1 have intact IFN-antagonistic properties, evident by the failure to upregulate IFN-stimulated gene (ISG) protein expression (Supplementary Fig. 4g), allowing us to specifically test the autophagy function of TRIM23 in virus restriction. The replication of WT HSV-1 was similar for WT and *TRIM23* $^{-/-}$ MEFs, likely due to the strong autophagy-antagonistic capacity of this virus. However, the replication of mutHSV-1, which is impaired in autophagy antagonism, was enhanced by almost 2-log in *TRIM23* $^{-/-}$ MEFs as compared to WT cells, indicating that the autophagy function of TRIM23 confers antiviral activity (Fig. 2h). To corroborate these findings, we tested the replication capacity of Ad-GFP and SINV, both of which are known to be restricted by autophagy[23,24], in WT and *TRIM23* $^{-/-}$ MEFs. As compared to WT MEFs, *TRIM23* $^{-/-}$ cells exhibited markedly enhanced replication of Ad-GFP and SINV (Fig. 2i,j). Taken together, these results indicate that TRIM23 plays a central role in virus-triggered autophagy, and this activity of TRIM23 restricts viruses that are targeted by autophagy for degradation.

K27-linked auto-polyubiquitination of the ARF domain is required for TRIM23-mediated autophagy

A key feature of TRIM proteins is their N-terminal RING-finger E3 ligase activity, which mediates the conjugation of ubiquitin or ubiquitin-like proteins. In addition, TRIM proteins have different C-terminal domains, which typically mediate protein-protein interactions, but can also have enzymatic activity[1]. TRIM23 is unique in that it is the only TRIM family member that possesses a C-terminal ARF domain, which has GTPase activity[25]. To determine the relevance of the RING and ARF domains for TRIM23-mediated autophagy, we tested mutant proteins of TRIM23 in which these two domains have been deleted individually (ΔRING and ΔARF TRIM23) for their ability to induce GFP-LC3B puncta. Whereas ectopic expression of WT TRIM23 robustly triggered GFP-LC3B puncta formation, the ΔRING and ΔARF TRIM23 mutants did not (Fig. 3a–c). To test if the enzymatic activity of the RING domain is important for TRIM23 autophagy function, we generated a C34A mutant of TRIM23, which is defective in E3 ligase activity[18,26]. Similar to the ΔRING mutant, the TRIM23 C34A mutant completely lost the ability to induce GFP-

LC3B puncta (Fig. 3b,c). This indicates that both the RING E3 ligase activity and the ARF domain are required for TRIM23-mediated autophagy.

During our studies, we noticed several higher molecular weight bands of FLAG-TRIM23, which immunoblotting confirmed as polyubiquitinated versions of TRIM23 (Fig. 3d). Interestingly, rapamycin treatment enhanced the ubiquitination of FLAG-TRIM23 (Supplementary Fig. 5a). Consistent with these results, we also readily detected polyubiquitination of endogenous TRIM23, which was minimal under normal conditions, but strongly increased upon autophagy induction by rapamycin (Fig. 3e). To determine whether TRIM23 ubiquitination represents auto-ubiquitination or is mediated by the activity of another E3 ligase, we compared the ubiquitination levels of WT TRIM23 with those of the catalytically-inactive TRIM23 mutants, ΔRING and C34A. Unlike WT TRIM23, the ΔRING and C34A TRIM23 mutants had no detectable ubiquitination (Fig. 3d), strongly suggesting that TRIM23 is auto-ubiquitinated. Furthermore, the ΔARF mutant of TRIM23 also showed a near-complete loss of polyubiquitination (Fig. 3f and Supplementary Fig. 5b).

To identify the lysine residues in TRIM23 that undergo ubiquitination, we performed large-scale affinity purification of FLAG-TRIM23 expressed in mutHSV-1-infected HEK293T cells, and then analyzed the ubiquitinated TRIM23 bands by mass spectrometry (MS). This identified six ubiquitination sites in TRIM23: K250 located in the coiled-coil (CC) domain, and K402, K425, K446, K458 and K460 located in the ARF domain (Supplementary Fig. 5c), suggesting that the ARF domain is the major site of ubiquitination. Individual mutations of K250, K402, K425, and K446 to arginine, and double mutation of K458 and K460 to arginine, all failed to detectably diminish the ubiquitination levels of TRIM23 (Supplementary Fig. 5d); however, combined mutation of the five lysines located in the ARF domain (K402R/K425R/K446R/K458R/K460R; hereafter referred to as TRIM23 5K→R) led to a near-complete loss of TRIM23 ubiquitination, similar to ΔARF TRIM23 (Fig. 3f).

To determine whether ubiquitination of the ARF domain is required for TRIM23's autophagy function, we tested WT TRIM23 and its 5K→R mutant for their ability to induce autophagy. Whereas WT TRIM23 expression led to high numbers of GFP-LC3B puncta, the 5K→R mutant lost this ability, similar to the ΔARF TRIM23 mutant (Fig. 3g and Supplementary Fig. 5e). Collectively, these results indicate that auto-ubiquitination of TRIM23 at K402, K425, K446, K458 and K460 is required for the autophagy-promoting activity of TRIM23.

To identify the linkage type of TRIM23 auto-polyubiquitination, we expressed in HEK293T cells FLAG-TRIM23 together with HA-tagged WT ubiquitin (WT Ub), or Ub mutants in which all internal lysines are mutated except one (Fig. 3h). Co-expression of WT Ub as well as the Ub-K27only and Ub-K29only mutants led to efficient TRIM23 polyubiquitination, while co-expression of other Ub mutants did not (Fig. 3h). To corroborate this, we performed an *in vitro* restriction assay utilizing a set of deubiquitinating (DUB) enzymes that remove specific ubiquitin linkage types[27] (Fig. 3i): OTUB1 (K48-linkage-specific), OTUB2 (K63-linkage-specific), TRABID (K29- and K33-linkage-specific), and YOD1 (K27-, K29- and K33-linkage specific). USP21, which cleaves all types of ubiquitin linkages, served as positive control in this assay. Incubation with YOD1 and USP21

profoundly reduced the ubiquitination of FLAG-TRIM23, while other DUB enzymes had no effect (Fig. 3i,j). Moreover, co-expression of TRIM23 with WT Ub, but not a K27R Ub mutant, led to efficient TRIM23 polyubiquitination (Fig. 3k), providing further evidence that TRIM23 is primarily modified by K27-linked polyubiquitination. Collectively, these results indicate that K27-linked auto-polyubiquitination of TRIM23 at the C-terminal ARF domain is required for TRIM23 autophagy function.

K27-linked ubiquitination is required for the GTPase activity of TRIM23 and its recruitment to autophagosomal membranes

The ARF domain of TRIM23 has been shown to have GTP hydrolysis activity *in vitro*[25], but the relevance of this activity for TRIM23 function during viral infection remains unknown. Interestingly, homology modeling of the TRIM23 ARF domain based on the crystal structure of ARF6 revealed that the five ubiquitinated lysine residues are in close proximity to the GTPase catalytic site, and located in regions that undergo major structural changes during the GDP-GTP cycle (Fig. 4a). Therefore, we next asked whether *1.)* GTP hydrolysis activity is required for TRIM23 autophagy function; *2.)* GTPase activity affects TRIM23 ARF ubiquitination; or, alternatively *3.)* K27-linked ubiquitination affects the GTPase enzymatic activity. In contrast to WT TRIM23, a mutant of TRIM23 that has abolished GTP hydrolysis activity (TRIM23 K458I)[25] did not induce GFP-LC3B puncta formation, similar to the ΔARF TRIM23 mutant (Fig. 4b), suggesting that GTPase activity is required for TRIM23-mediated autophagy.

The TRIM23 K458I mutant had comparable ubiquitination levels as WT TRIM23, suggesting that GTPase activity is not a prerequisite for TRIM23 auto-ubiquitination (Supplementary Fig. 6a). To test whether K27-linked ubiquitination affects the GTP hydrolysis activity of TRIM23, we performed a luciferase-based *in vitro* GTPase assay using purified TRIM23 WT and 5K→R mutant proteins (Fig. 4c). WT TRIM23 showed efficient GTPase activity, which was similar to that of Rab5α, a distantly related small GTPase of the Rab protein family. In contrast, the TRIM23 5K→R mutant exhibited low GTPase activity, comparable to that of the GTPase-defective mutants K458I and ΔARF. Importantly, the C34A mutant, which has abolished RING E3 ligase activity, also showed defective GTPase activity (Fig. 4c), further strengthening that TRIM23 auto-ubiquitination is important for GTPase activity. In accord, an *in vitro* GTPase assay measuring free phosphate production showed that, unlike WT TRIM23, the TRIM23 5K→R, C34A, K458I and ΔARF mutants had strongly impaired GTP hydrolysis activities (Supplementary Fig. 6b). Next, as GTPase-defective TRIM23 mutants are expected to exhibit prolonged GTP-bound states, we tested purified WT TRIM23 and its 5K→R mutant for their abilities to bind GTP-agarose matrix *in vitro*. In this assay, the TRIM23 mutant K458I, which is locked in the GTP-bound state, as well as ΔARF TRIM23, which is unable to bind GTP, served as controls (Fig. 4d). TRIM23 5K→R bound to GTP-agarose more strongly than did WT TRIM23, which supports the conclusion that ubiquitination of the ARF domain is important for its GTP-GDP cycling activity, and also indicates that the 5K→R mutation does not perturb the overall ARF structure (Fig. 4d). To further strengthen these data, we purified FLAG-TRIM23 WT from cells in which either WT Ub, or the Ub mutants K27R or K27only were overexpressed, and then measured TRIM23 GTPase activity *in vitro* (Fig. 4e). This showed that TRIM23

purified from WT Ub or K27only Ub expressing cells exhibited strong GTP hydrolysis activity, but not TRIM23 from cells transfected with K27R Ub. These results indicate that K27-linked auto-ubiquitination of TRIM23 at the ARF domain is important for its GTPase enzymatic activity.

The ARF domain of TRIM23 is highly homologous in sequence to members of the ARF protein family of small GTPases (ARF1–6) (Supplementary Fig. 6c), which are important regulators of membrane trafficking and organelle structures[28]. A common feature of ARF proteins and other small GTPases is their ability to cycle between the cytosol and membrane structures, or between different membrane compartments (*e.g.* Golgi and late endoplasmic reticulum) in a GTP hydrolysis-dependent manner[29]. Therefore, we tested whether the GTPase activity of TRIM23 is necessary for its recruitment to p62-containing autophagosomal membranes. Whereas WT TRIM23 co-localized extensively with endogenous p62 punctate structures, the 5K→R, K458I, and C34A mutants showed much less co-localization (Fig. 4f). We further observed that, compared to WT TRIM23, the K458I, 5K→R, and C34A mutants exhibited a more punctate localization in vesicles that did not co-localize with p62 (Fig. 4f), suggesting that K27-polyubiquitin-dependent GTPase activity is needed for the cycling of TRIM23 from intracellular compartments (*e.g.* the Golgi as previously reported[30]) to autophagosomes. We next addressed whether TRIM23 co-localizes to early autophagosomes in a GTPase-dependent manner by determining its co-localization with the early autophagosomal marker ATG16L[31]. Whereas WT TRIM23 co-localized with ATG16L-positive vesicles, the K458I and 5K→R mutants did not show co-localization with ATG16L (Supplementary Fig. 6d,e). Moreover, neither WT TRIM23 nor the K458I and 5K→R mutants co-localized with the lysosomal marker LAMP1 (Supplementary Fig. 6f). Taken together, these data indicate that K27-linked ubiquitination is essential for TRIM23 enzymatic activity to hydrolyze GTP, and that the ubiquitin-dependent GTPase activity promotes the recruitment of TRIM23 to early autophagosomal membranes.

Interaction of TRIM23 with TBK1 and p62 during autophagy

To identify the molecular mechanism of TRIM23 in virus-induced autophagy, we sought to identify the TRIM23 interactome through MS analysis of cellular factors that co-purified with FLAG-TRIM23 from mutHSV-1-infected HEK293T cells. We found TBK1 and p62, two key molecules in selective autophagy[10,11,19,32], as major TRIM23 interaction partners (Supplementary Fig. 7a). We first confirmed the interaction of TRIM23 with TBK1 and p62 by co-immunoprecipitation (co-IP) and found that, whereas binding of endogenous TRIM23 to TBK1 and p62 was minimal in uninfected cells, the interaction was induced by mutHSV-1 infection (Fig. 5a,b). Moreover, autophagy stimulation by rapamycin also enhanced TRIM23 binding to TBK1 and p62 (Fig. 5a,b). Confocal microscopy showed that ectopically expressed V5-TRIM23 co-localized extensively with both GFP-p62 and FLAG-TBK1 even without stimulation of autophagy; in contrast, endogenous TRIM23, TBK1 and p62 co-localized specifically upon autophagy stimulation, but not under normal (unstimulated) conditions (Supplementary Fig. 7b,c). In accord, co-IP also indicated that endogenous TRIM23 forms a ternary complex with endogenous TBK1 and p62 specifically in mutHSV-1-infected or rapamycin-treated cells, but not mock-treated cells, suggesting that

their interaction is inducible (Supplementary Fig. 7d). *In vitro* binding assay using purified GST-TRIM23 and His-tagged TBK1 proteins showed an efficient interaction, suggesting that TBK1 is a direct binding partner of TRIM23 (Supplementary Fig. 7e). Mapping studies by co-IP revealed that WT TRIM23, but not the ΔARF mutant of TRIM23, bound to endogenous TBK1 and p62 (Fig. 5c). Notably, the 5K→R mutant bound to TBK1 and p62 as efficiently as WT TRIM23, indicating that the K27-linked ubiquitination of the ARF domain is not necessary for recruiting TBK1 and p62 to TRIM23. Finally, complementary binding studies using truncated TBK1 constructs showed that TRIM23 interacted with the N-terminal kinase domain (KD) of TBK1, but not with its central ubiquitin-like domain (ULD) or C-terminal coiled-coil (CC) domains (Fig. 5d,e).

We next asked whether TBK1 and p62 are required for TRIM23-mediated autophagy. Individual depletion of endogenous TBK1 or p62 markedly reduced the numbers of GFP-LC3B puncta induced by ectopically expressed FLAG-TRIM23, while transfection of non-targeting control siRNA (si.NT) did not have any effect (Fig. 5f,g). Treatment with the TBK1 inhibitor BX795[33] abrogated the conversion of endogenous LC3B-I to LC3B-II induced by FLAG-TRIM23 (Fig. 5h), suggesting that the catalytic activity of TBK1 is necessary for TRIM23-mediated autophagy. Together, these results indicate that upon autophagy stimulation TRIM23 forms a complex with TBK1 and p62, and further that the kinase activity of TBK1 is important for mediating TRIM23's function in autophagy.

TRIM23 GTPase-dependent activation of TBK1 to phosphorylate p62

Recent studies demonstrated that during mitophagy or bacterial infection, TBK1 phosphorylates p62 at S403 and several other residues, thereby facilitating p62-mediated autophagic clearance[10,11,34]. We therefore hypothesized that TBK1 phosphorylates p62 also during viral infection, and that this activity may be facilitated by TRIM23. Immunoblotting with a phospho-S403-specific p62 antibody showed detectable p62 phosphorylation upon mutHSV-1 infection or rapamycin treatment in control siRNA-transfected cells; in contrast, p62 phosphorylation was minimal in infected or rapamycin-stimulated cells that have been depleted of endogenous TRIM23 (Fig. 6a,b). Conversely, ectopic expression of FLAG-TRIM23 increased S403 phosphorylation of endogenous p62, an effect that was nullified by treatment of cells with BX795 (Fig. 6c). To test if TRIM23 directly activates TBK1, we monitored by immunoblotting the *trans*-autophosphorylation of S172 in the activation loop of TBK1, which is indicative of TBK1 activation. We found that overexpressed TBK1 was already partially autophosphorylated at S172 as previously reported[35], and co-expression of V5-TRIM23 strongly enhanced TBK1 autophosphorylation (Fig. 6d). Confocal microscopy experiments showed that exogenously expressed TRIM23 also readily induced phosphorylation of endogenous TBK1 at S172, and it co-localized with phospho-S172-TBK1 in cytoplasmic punctate structures that also stained for p62 (Fig. 6e).

Our data indicated that K27-linked autoubiquitination of the ARF domain is important for TRIM23 GTPase activity and autophagy function. Thus, we next asked whether K27-ubiquitination and GTPase activity are important for TBK1 activation by TRIM23. In contrast to WT TRIM23, the mutants 5K→R and K458I failed to enhance TBK1 phosphorylation at S172 as compared to vector transfection (Fig. 6f). In accord, ectopic

expression of WT TRIM23 but not of the mutants 5K→R and K458I triggered endogenous p62 degradation, indicative of increased autophagic flux (Fig. 6f). Furthermore, the TRIM23 ΔARF mutant, which did not bind TBK1 or co-localize with LC3B-positive autophagosomes (Fig. 5f and Supplementary Fig. 8a), also did not promote TBK1 S172 autophosphorylation or p62 degradation (Fig. 6f). In line with these results, whereas WT TRIM23 effectively restricted mutHSV-1 infection, the TRIM23 mutants 5K→R and ΔARF failed to block virus replication (Supplementary Fig. 8b).

Finally, we asked how TRIM23 binding leads to activation of TBK1 in a manner that is dependent on its GTPase activity. As TBK1 enzymatic activation is known to require dimerization or higher-order oligomerization to allow *trans*-auto-phosphorylation at S172 to occur[36–38], we tested whether the GTPase activity of TRIM23 facilitates TBK1 self-association by measuring the extent to which HA-tagged TBK1 co-purified with GST-TBK1. In the presence of WT TRIM23, we observed an increase in the amounts of co-purifying HA-TBK1, but not in the presence of the GTPase-defective mutants 5K→R and K458I or vector transfection control (Fig. 6g). Collectively, these results suggest that TRIM23's ARF GTPase activity induces TBK1 activation by promoting self-association of the kinase.

DISCUSSION

Over the past decade, it has become clear that members of the TRIM E3 ligase family are important players in innate immune surveillance pathways[1]. More recently, a growing number of studies indicated that TRIM proteins also regulate autophagy in response to viral infection or non-viral autophagy stimuli[14,39,40]. In this study, we tested the role of multiple TRIM proteins in the autophagic response to viral pathogens (both RNA and DNA viruses) from three major virus families. While some TRIM proteins were required for autophagy upon both RNA and DNA virus infection, others were critical for autophagic flux in response to one particular type of viral pathogen. Interestingly, for the latter group of TRIM proteins, their virus-specific roles in autophagy correlated with their functions in intracellular innate immune responses to that particular virus. For example, TRIM56, which is known to regulate STING-dependent sensing of HSV-1 infection[41], was required for autophagy induction in response to infection by HSV-1, but not the RNA viruses IAV and EMCV. TRIM25, which activates the sensor RIG-I via K63-polyubiquitin[42], specifically regulated autophagy in response to IAV, known to be sensed by RIG-I. Furthermore, TRIM13, which regulates EMCV-induced IFN induction by the sensor MDA5[43], was also essential for EMCV-triggered autophagy. These correlations suggest that the functional roles of TRIM proteins in innate signaling and autophagy to a specific viral pathogen are intricately connected. In light of recent evidence suggesting that TRIM proteins can act as specific autophagy receptors by recognizing viral components[14], future studies will need to determine the molecular details of how TRIM proteins link innate immune recognition and autophagy, and which viral (or host) features are recognized by TRIM proteins to trigger autophagy.

We also identified a few TRIM proteins, including TRIM23, which had a profound effect on autophagy triggered by both RNA and DNA viruses as well as rapamycin, suggesting that

these TRIM proteins regulate a fundamental step in the autophagic process. Our mechanistic studies revealed that TRIM23 is a core component of selective autophagy by assembling a signaling complex composed of the autophagy receptor p62 and its upstream regulator TBK1, ultimately promoting TBK1-mediated p62 phosphorylation and thereby autophagy. Our data thus identify the TRIM23-TBK1-p62 ternary complex as an important component of virus-induced autophagy. As rapamycin also induced the interaction of TRIM23 with TBK1 and p62, it is likely that the TRIM23-TBK1-p62 complex also regulates autophagy in non-viral contexts. Future studies will need to define the upstream stimuli and molecules that activate TRIM23 during autophagy, which may also reveal the molecular details of how TRIM23 functions specifically in p62-mediated selective autophagy, but not starvation-induced autophagy. Furthermore, whereas our study demonstrated that TRIM23-mediated autophagy restricts HSV-1, SINV and Ad, which are known to be targeted for degradation by autophagy[6–8], the role of TRIM23-induced autophagy in the life cycle of viruses that usurp autophagy for their efficient replication remains to be addressed. Moreover, as TRIM23 reportedly has both positive and negative regulatory roles in the antiviral type I IFN response[21,22], in-depth studies are required to identify the molecular details of how TRIM23 dually coordinates virus-induced autophagy and IFN responses.

TRIM23 is unique among the ~80 TRIM proteins in that it harbors both E3 ligase and GTPase enzymatic activities. We found that K27-linked auto-polyubiquitination of the ARF domain was required for TRIM23 GTP hydrolysis activity. Structure modeling indicated that the five ubiquitinated lysine residues are located in regions in the TRIM23 ARF domain that undergo extensive structural changes during the GDP-GTP cycle. It is thus conceivable that ubiquitin chains conjugated to the TRIM23 ARF sterically lock it in the active conformation, or alternatively, make the enzymatically-inactive conformation of TRIM23 less favorable. As unconventional ubiquitin chains have been shown to also serve as recruitment platforms for protein interactions, it is also possible that K27-linked polyubiquitin allows for binding of host factors, such as GTPase-activating proteins, which promotes TRIM23 GTPase activity. Furthermore, it will be important to test whether other small GTPases also undergo non-degradative polyubiquitination for their enzymatic activity.

The GTP hydrolysis activities of ARF proteins and other small GTPases have been shown to allow cytosol-membrane or membrane-membrane cycling of these enzymes. Our study revealed that the GTPase activity of TRIM23 is needed for the localization of TRIM23 to autophagosomal membranes, to activate TBK1 there, thereby promoting phosphorylation of the autophagic receptor p62. Biochemical characterization showed that TRIM23 binds with its C-terminal ARF domain to the N-terminal KD of TBK1, and that GTP hydrolysis activity of the ARF stimulates TBK1-mediated phosphorylation of p62 at S403 in its ubiquitin-associated (UBA) domain, which was shown to promote cargo recruitment and autophagic flux[32,34,44,45]. Our data support a model in which TRIM23 binding to the N-terminal KD of TBK1, and likely conformational changes induced by GTP-GDP cycling of its ARF domain, induce TBK1 dimer/multimer formation in a manner that facilitates TBK1 auto-phosphorylation of the activation loop in *trans.*

Besides TBK1 autophosphorylation, direct non-degradative ubiquitin modification of TBK1 was shown to be important for its activation in the IFN induction pathway, and multiple E3

ligases, including MIB1/2, have been implicated in TBK1 ubiquitination[37,46,47]. We observed modification of TBK1 with polyubiquitin upon exogenous expression of WT TRIM23, but not its E3 ligase-defective C34A mutant, to a similar extend as seen in the presence of MIB2, which served as a positive control (Supplementary Fig. 8c). Chemical inhibition of the proteasome did not enhance TBK1 ubiquitination induced by TRIM23 (Supplementary Fig. 8d), suggesting that TRIM23 promotes non-degradative ubiquitination of TBK1, likely indicative of TBK1 activation. However, the role of TBK1 ubiquitination for virus-induced autophagy warrants further investigation, and whether TBK1 is a direct substrate of TRIM23-mediated ubiquitination.

Taken together, our work unveils a role for K27-linked ubiquitination in TRIM23 GTPase function and its ability to activate TBK1-mediated autophagy, which may provide the basis for therapeutics against diseases caused by dysregulation of autophagy, such as microbial infections, inflammation, and cancer.

METHODS

Cell Culture and Viruses

HEK293T, Vero, and HeLa cells (all purchased from ATCC) as well as WT and *ATG5* $^{-/-}$ MEF cells[17] and HeLa cells stably expressing GFP-LC3B[48,49] (kindly provided by Wen-Xing Ding, University of Kansas Medical Center) were cultured in Dulbecco's Modified Eagle's Medium (DMEM; Life Technologies) supplemented with 10% (v/v) fetal bovine serum (FBS; Hyclone), 1% (v/v) Penicillin-Streptomycin (Life Technologies) and 1% (v/v) L-Glutamine (Life Technologies). *TRIM23* $^{+/+}$ and *TRIM23* $^{-/-}$ MEFs[18] were propagated in DMEM (Life Technologies) supplemented with 10% (v/v) Mesenchymal Stem Cell Growth Medium (LONZA), 1% (v/v) L-Glutamine (Life Technologies), and 1% (v/v) Penicillin-Streptomycin (Life Technologies). BHK-21 cells (ATCC) were maintained in Eagle's Minimum Essential Medium (EMEM; ATCC) supplemented with 10% (v/v) fetal bovine serum (FBS; Hyclone) and 150 μL/L Gentamicin (Life Technologies).

TRIM23 $^{-/-}$ MEFs were verified by immunoblotting with anti-TRIM23 antibody to confirm absence of TRIM23 protein expression. Cell lines from ATCC were authenticated by ATCC and were not validated further in our laboratory. Cell lines that were obtained and validated by other groups were not further authenticated. All cell lines used in this study have been regularly tested for potential mycoplasma contamination.

HSV-1 WT and mutant γ34.5 virus (mutHSV-1; previously termed Δ68H-6) were provided by S. Rabkin (Harvard) and have been previously described[16]. IAV (strain PR8/34 H1N1) was a gift from A. García-Sastre (Icahn School of Medicine at Mount Sinai). RSV (A2 strain) and EMCV (EMC strain) were purchased from ATCC. Sendai virus (Cantell strain) was purchased from Charles River Laboratories. Ad-GFP was obtained from Vector Biolabs (#1060) and SINV (strain HRSP) was generously provided by R. Kuhn (Purdue University).

Plasmids and Transfections

The TRIM cDNA library (HA-tagged and V5-tagged) was kindly provided by A. García-Sastre (Icahn School of Medicine at Mount Sinai) and J. Jung (University of Southern

California) and has been described previously[2]. pCMV6-TRIM23-MYC-DDK was purchased from Origene (NM_001656) and used as a PCR template to generate the truncation mutants TRIM23 ΔRING (aa 77–574) and TRIM23 ΔARF (aa 1–390) cloned into the pCMV6-MYC-DDK vector using BamHI and MluI. Point mutations in pCMV6-TRIM23-MYC-DDK were introduced by site-directed mutagenesis (Phusion Flash, New England Biolabs) to generate the TRIM23 mutants C34A, K458I, K250R, K402R, K425R, K446R, and K458R/K460R. The cDNA of the TRIM23 5K→R (K402R/K425R/K446R/K458R/K460R) mutant was purchased from GeneART (Thermo Fisher Scientific) and subcloned into the pCMV6-MYC-DDK-vector using BamHI and NotI restriction sites. TRIM23-V5 was constructed by subcloning full-length TRIM23 into the pEF-IRES-puro vector using XbaI and XhoI sites. pLKO.1-sh.NT (Sense sequence: CCTAAGGTTA AGTCGCCCTC GCTCGAGCGA GGGCGACTTA ACCTTAGG) and pLKO.1-sh.TRIM23 (Sense sequence: GCAGTCATAG AGACAGAATTA) were purchased from Open Biosystems. pCMV6-RAB5A-MYC-DDK was acquired from Origene (NM_004162). The 3×FLAG-pCMV-p62 construct was provided by Y. Feng (Washington University, St Louis) and has been described previously[50]. pEGFP-C1-LC3 and pEGFP-1-p62 were described previously[20,51]. MIB2-FLAG[46] (Addgene #37117) as well as pCMV3-3×FLAG-hTBK1 (aa 1–729), pCMV3-3×FLAG -TBK1ΔCC (aa 1–385), pCMV3-3×FLAG -TBK1ΔULD and pCMV3-3×FLAG -TBK1-KD (aa 1–305) were kindly provided by M. Dorf (Harvard) and have been previously described[52]. pIRES-TBK1CC (aa 384–729) −3×FLAG was generated by subcloning the cDNA encoding aa 384–729 of TBK1, including a C-terminal 3×FLAG tag, into the pEF-IRES-puro vector using XhoI and EcoRI restriction sites. GST-TBK1 was generously provided by C. Joo (University of Ulsan College of Medicine, South Korea). HA-tagged Ub-WT (#17608) and mutants K33-only-Ub (#17607), K48-only-Ub (#17605), and K63-only-Ub (#17606) cloned into the pRK5-HA vector were a kind gift from T. Dawson (Addgene,[53]). HA-tagged K6-only-Ub (#22900), K11-only-Ub (#22901), K27-only-Ub (#22902), and K29-only-Ub (#22903) were provided by S. Weller (Addgene,[54]). HA-tagged K27R-Ub was generated by site-directed mutagenesis using pRK5-HA-ubiquitin WT as template. pmRFP-LC3(#21075) was a gift from T. Yoshimori (Addgene,[55]). All constructs were sequenced to verify 100% agreement with the original sequence. Transfections were performed using the calcium phosphate method, or using Lipofectamine LTX and Plus reagent (Life Technologies), or linear polyethylenimine (1 mg/mL solution in 20 mM Tris pH 6.8; Polysciences Inc.) according to the manufacturer's instructions.

Antibodies and Reagents

For immunoblot analysis, the following antibodies were used: α-FLAG (1:2,000, M2, Sigma), α-HA (1:2,000, HA-7, Sigma), α-V5 (1:5,000, R960-25, Novex), α-GST (1:5,000, Sigma or 1:1,000, NB600-325, Novus Biologicals), α-β-actin (1:10,000, AC-15, Sigma), α-TRIM23 (1:1,000, ab97291, Abcam), α-ubiquitin (1:500, P4D1, Santa Cruz), α-LC3 (mouse, LC3.No.6, 1:1,000, Cosmo Bio USA), α-LC3B (rabbit, 1:1,000, NB100-2220, Novus Biologicals), α-p62 (1:2,000, α-N-term, PROGEN Biotechnik), α-TBK1 (1:2,000, 3013, Cell Signaling), α-ICP8 (1:5,000, kindly provided by D. Knipe, Harvard), α-phospho-S403-p62 (1:500, Cell Signaling), α-SeV (1:2,000, PD029, MBL), α-ISG15 (1:1,000, Santa Cruz, F-9), α-3Dpol (1:400, 3B7, Santa Cruz), α-SINV (1:500, V-560-701-562, ATCC), α-RIG-I (1:1,000, Alme-1, LSBio) and α-phospho-S172-TBK1 (1:1,000, 5483, Cell

Signaling). For immunoprecipitation of TRIM23, α-TRIM23 (ab97291, Abcam) was used. For immunoprecipitation of FLAG-tagged constructs, α-FLAG M2 Affinity Gel or magnetic beads (both Sigma), or α-FLAG antibody (M2, Sigma) and Protein A/G agarose (Thermo Fisher) were used.

Pepstatin A and E64D (used at 10 μg/mL for 2–4 h; Sigma) were used to block autophagic flux in the experiments that assessed endogenous LC3B-I to LC3B-II conversion or GFP-LC3B puncta formation upon mutHSV-1 infection, rapamycin treatment, or ectopic expression of TRIM proteins. Rapamycin (used at 100 – 150 nM [MEFs] or 3 μM [HEK293T and HeLa]) was purchased from Sigma. BX795 (used at 1 μM) was purchased from Santa Cruz. Recombinant IFNα_2 was obtained from PBL Biomedical Laboratories. MG132 (M8699), phosphatase inhibitor cocktail (P5726) and protease inhibitor cocktail (P2714) were purchased from Sigma and used at 50 μM, 1:100 and 1:500 respectively.

Confocal Microscopy

HEK293T, HeLa, or MEF cells were grown in chamber slides (Thermo Fisher), or on cover slips (Chemglass) in 24-well plates, and transfected and/or infected as indicated. Cells were fixed with 4% (w/v) paraformaldehyde (PFA, Santa Cruz) for 20 min, permeabilized with 0.5% (v/v) Triton-X-100 in PBS, and then blocked with 10% (v/v) goat serum or 1% milk powder in PBS for 1 h. For immunostaining, α-TRIM23 (1:200, ab97291, Abcam), α-LC3 (1:400, Novus Biologicals), α-phospho-S172-TBK1 (1:400, 5483, Cell Signaling), α-TBK1 (1:400, #3013, Cell Signaling), α-TRIM23 (1:100, clone C-1, sc-393923, Santa Cruz), α-FLAG (1:400, M2, Sigma), α-p62 (1:400, PROGEN Biotechnik), α-LAMP1 (1:400, H4A3, Developmental Studies Hybridoma Bank), α-V5 (1:500, R960-25, Life Technologies), α-myc (1:400, 9B11, Cell Signaling) and α-ATG16 (1:200, A7356, Sigma) were used, followed by incubation with secondary antibodies conjugated to Alexa Fluor 488, Alexa Fluor 555, Alexa Fluor 594, Alexa Fluor 633, or Alexa Fluor 647 (all 1:400, Life Technologies). Cells were mounted in DAPI-containing Vectashield (Vector Labs) to co-stain nuclei. All laser scanning images were acquired on an Olympus IX8I confocal microscope or on a Leica SP8 confocal microscope. Cytoplasmic GFP-LC3B puncta in HeLa, HEK293T and MEF cells were manually counted for 30 or 50 randomly selected cells.

TRIM cDNA screen for autophagy induction

2×10^5 HeLa cells, grown on 12 mm-glass cover slips (Chemglass) in 24-well plates, were transiently transfected with GFP-LC3B (500 ng) and either empty vector plasmid (control) or plasmids encoding the individual TRIM proteins (V5- or HA-tagged, 1500 ng) using FuGENE reagent (Roche) according to the manufacturer's protocol. At 48 h post-transfection, cells were treated with 10 μg/mL Pepstatin A and E64D for 3 h to block autophagic flux. Stimulation of cells with rapamycin (3 μM) for 2 h served as positive control. Cells were rinsed once with PBS and fixed in 4% (w/v) PFA (Santa Cruz) for 20 min at room temperature. Fixed cells were mounted on glass slides using the Vectashield HardSet mounting medium including DAPI to visualize cell nuclei. GFP-LC3B puncta for 30 randomly selected cells were quantified using an Olympus IX8I confocal laser scanning

microscope. In parallel, expression of the individual TRIM proteins was confirmed by IB analysis.

In Vitro DUB Restriction Assay

Purified human DUB enzymes were purchased from Thermo Fisher Scientific: USP21 (DB509), OTUB1 (H00055611-P01), OTUB2 (C242), YOD1 (NBP2-22955), and Trabid (E-560). HEK293T cells overexpressing FLAG-TRIM23 and HA-Ub WT were lysed in NP-40 buffer (150 mM NaCl, 1% [v/v] NP-40, 50 mM HEPES pH 7.4, and protease inhibitor cocktail [Sigma]) at 48 h post-transfection, and cell debris pelleted by centrifugation at 13,000 rpm for 20 min at 4 °C. Post-centrifuged WCLs were incubated with FLAG M2 magnetic beads (Sigma) for 4 h. FLAG-precipitates were washed extensively with 500 mM NaCl-containing NP40 lysis buffer and then incubated in DUB assay buffer (25 mM Tris, pH 7.5, 150 mM NaCl, 4 mM Dithiothreitol [DTT]) together with 2 μg of recombinant USP21, OTUB1, OTUB2, YOD1, or Trabid at 37 °C for 2 h. The reaction was stopped by adding Laemmli SDS sample buffer and heating at 95 °C for 5 min. Samples were separated by SDS-PAGE, and polyubiquitination of TRIM23 was determined by IB with α-HA antibody.

In Vitro Binding Assay

Purified recombinant human His-TBK1 (H00029110-P01), GST-TRIM23 (H00000373-P01) and GST (NBP1-30259) were purchased from Novus Biologicals. Glutathione Agarose Beads (Pierce #78601) were incubated with 0.5 μg GST-TRIM23 or GST in Triton X-100 buffer (150 mM NaCl, 5 mM EDTA, 1% [v/v] Triton X-100, 50 mM HEPES pH 7.4, and protease inhibitor cocktail [Sigma]) for 16 h at 4 °C. Beads were washed extensively to remove unbound protein, and subsequently incubated with 0.5 μg His-TBK1 in Triton X-100 buffer for 4 h at 4 °C. Beads were washed extensively and elution of precipitated proteins was performed by heating samples in Laemmli SDS sample buffer at 95 °C for 5 min, followed by SDS-PAGE.

GTP-Agarose Pulldown

HEK293T cells (~ 6×10^6 cells per sample), transiently transfected with vector, FLAG-tagged TRIM23 WT or mutants, were lysed in 1000 μL GTP binding buffer (20 mM Tris-HCl pH 7.5, 5 mM $MgCl_2$, 150 mM NaCl, 0.1% [v/v] Triton X-100, and protease inhibitor cocktail [Sigma]), and cell lysates were cleared from cell debris by centrifugation at 13,000 rpm for 20 min at 4 °C. Post-centrifuged lysates were mixed with a ~50% slurry of GTP agarose resin (Novus Biologicals, 505-0001) and incubated for 2 h at 4 °C. After extensive washing of the beads with GTP binding buffer, samples were boiled in Laemmli SDS sample buffer for 5 min at 95 °C, followed by SDS-PAGE.

TRIM RNAi Screen

HeLa cells stably expressing GFP-LC3B[48] were seeded into 24-well plates (~ 2.5×10^5 cells per well) on glass cover slips (Chemglass). 16 h later, cells were transfected with 40 nM of non-targeting scrambled siRNA (si.NT), or siRNAs targeting individual TRIM or ATG genes using Lipofectamine RNAiMAX (Invitrogen) according to the manufacturer's

instructions. The following Dharmacon siGENOME SMARTpool siRNAs were used: si.TRIM74 (M-031736-01), si.TRIM56 (M-007079-00), si.TRIM44 (M-017337-01), si.TRIM41 (M-007105-02), si.TRIM38 (M-006929-01), si.TRIM25 (M-006585-00), si.TRIM23 (M-006523-00), si.TRIM21 (M-006563-02), si.TRIM20 (M-011081-00), si.TRIM16 (M-012220-01), si.TRIM13 (M-006923-00), si.TRIM5 (M-007100-00), si.ATG5 (M-004374-04), si.ATG7 (M-020112-01), si.ATG12 (M-010212-02), and si.NT (siGenome Control Pool D-001206-14-50). 48 h later, autophagy was induced using the following stimuli: 3 μM rapamycin for 4 h; mutHSV-1 (MOI 4) for 8 h; EMCV (MOI 100) for 6 h; or IAV (MOI 5) for 14 h. As IAV and EMCV infection already causes a block of autophagic flux, only samples infected with mutHSV-1 or treated with rapamycin were additionally treated with E64D and Pepstatin A (each 10 μg/mL) for 4 h to inhibit autophagic flux. Cells were fixed in 4% (w/v) PFA (Santa Cruz) for 20 min at room temperature (RT), washed extensively with PBS, and mounted directly on glass slides for confocal microscopy analysis using the Vectashield HardSet mounting medium including DAPI to visualize cell nuclei. Laser scanning images were taken on an Olympus IX8I confocal microscope at a 40 × magnification. Using an Image J macro, the GFP-LC3B puncta were highlighted, the background eliminated and the image converted to a binary image (as shown in Supplementary Fig. 1c). The area of the highlighted GFP-LC3B puncta in an area of 500 × 500 pixels was quantified using ImageJ's particle analyzer function. A total of three data points (each 500 × 500 pixels, ~30 cells) were quantified from individual images for each screen. The whole screen was repeated three times. Data analysis, visualization and statistics (ANOVA two-way tests) were performed using custom R scripts.

SiRNA-mediated Knockdown of TBK1 and p62

HEK293T were seeded into 24-well plates (~ 2.5×10^5 cells per well). The next day, cells were transfected with 60 nM of gene-specific siRNAs using Lipofectamine RNAiMAX (Life Technologies) according to the manufacturer's instructions. SiRNAs targeting TBK1 (siGENOME SMARTpool M-003788-02-0005), or p62 (siGENOME SMARTpool M-010230-00-0005), as well as a non-targeting control siRNA (siGenome Control Pool D-001206-14-50) were purchased from Dharmacon. Forty-eight hours later, knockdown efficiency of endogenous TBK1 and p62 was determined by qRT-PCR as described below.

qRT-PCR Analysis

Total RNA was extracted from cells using the HP Total RNA Kit (OMEGA bio-tek) according to the manufacturer's instructions. Reverse transcription and qRT-PCR was performed in one step using 2 μl (~ 400 ng) of the purified RNA samples as templates (SuperScript III Platinum Kit, Invitrogen) on a 7500 Fast Real-Time PCR Machine (Applied Biosystems) according to the manufacturer's instructions. TaqMan probes for each individual gene were acquired as premixed master mixes (IDT) and added to the reaction. Expression level for each target gene was calculated by normalizing against *GAPDH* using the ΔΔCT method, and represented relative to the values for mock-treated cells, which were set to 1.

Analysis of TRIM23 mRNA Expression in Human Tissues

To determine the absolute copy number of TRIM23 transcripts in the Human Total RNA Master Panel II (Clontech), qPCR was performed in one step using 20 ng of the individual cDNA library samples and the SuperScript III Platinum Kit (Invitrogen) on a 7500 Fast Real-Time PCR Machine (Applied Biosystems) according to the manufacturer's instructions. A TaqMan probe for the TRIM23 gene was acquired as premixed (IDT) master mix and added to the reaction. A standard of known concentration was serially diluted to determine the absolute numbers of TRIM23 mRNA in the individual tissues.

Electron Microscopy

TRIM23$^{+/+}$ and *TRIM23*$^{-/-}$ MEF cells were grown in 6-well plates. Forty-eight hours later, cells were treated for 2 h with 10 μg/mL Pepstatin A/E64D and either mock-treated or treated with 150 nM rapamycin for 2 h, or infected with mutHSV-1 (MOI of 4) for 12 h. Cells were fixed with a mixture of 0.75% formaldehyde, 1.25 % glutaraldehyde and 0.015% picric acid in 50 mM sodium cacodylate buffer (pH 7.4) for 1 h at room temperature. After washing with sodium cacodylate buffer (50 mM pH 7.4), cells were scraped off, pelleted and embedded in Epon for 24 – 48 h at 40 °C. Perfused cells were cut ultrathin (Reichert-Ultracut-S) and transferred into a formvar/carbon coated copper grid for imaging. All images were acquired using the Tecnai G^2 Spirit BioTWIN (FEI) at the Electron Microscopy Facility of Harvard, Boston.

Pull-down Assay, Co-immunoprecipitation, and Immunoblot Analysis

HEK293T cells were lysed in Triton X-100 buffer (150 mM NaCl, 5 mM EDTA, 1% [v/v] Triton X-100, 50 mM HEPES pH 7.4, and protease inhibitor cocktail [Sigma]), NP-40 buffer (150 mM NaCl, 1% [v/v] NP-40, 50 mM HEPES pH 7.4, and protease inhibitor cocktail [Sigma]), or RIPA buffer (150 mM NaCl, 0.5 – 1% [v/v] NP-40, 1% [w/v] deoxycholic acid (DOC), 0.01% [v/v] SDS, 20 mM Tris pH 8.0, and protease inhibitor cocktail [Sigma]), and cell debris pelleted by centrifugation at 13,000 rpm for 20 min at 4 °C. FLAG pull-downs, Co-IP, and western blot analyses were performed as previously described[42]. Elution of precipitated proteins was performed by heating samples in Laemmli SDS sample buffer at 95 °C for 5 min.

Large-scale Protein Purification and Mass Spectrometry Analysis

To identify cellular interaction partners of TRIM23 in virus-infected cells, twenty 10cm-dishes of HEK239T cells (~ 1×10^7 cells per dish) were each transfected with 24 μg of pCMV6 empty vector or FLAG-TRIM23, followed by infection with mutHSV-1 (MOI 1) at 36 h post-transfection. 12 h later, cells were lysed with Triton X-100 buffer (150 mM NaCl, 5 % EDTA, 1% [v/v] Triton X-100, 50 mM HEPES pH 7.4, and protease inhibitor cocktail [Sigma]), followed by centrifugation at 13,000 rpm for 20 min at 4 °C. Post-centrifuged lysates were pre-cleared using 100 μl Sepharose® 4B (Sigma) to remove cell debris. Lysates were mixed with a ~50% slurry of α-FLAG M2 Affinity Gel (Sigma) and incubated for 4 h at 4 °C. After extensive washing of the beads with lysis buffer, bound proteins were eluted in 2× Laemmli SDS sample buffer for 5 min at 95 °C and separated on a NuPAGE 4–12% Bis-Tris gradient gel (Life Technologies). To stain co-immunoprecipitated proteins, a

Silverquest™ staining kit (Invitrogen) was used according to the manufacturer's instructions. Bands that were specifically present in the FLAG-TRIM23, but not empty vector, sample were excised and analyzed by ion-trap mass spectrometry analysis at the Harvard Taplin Biological Mass Spectrometry Facility, Boston.

To identify the lysine residues in TRIM23 which undergo ubiquitination, twenty 10cm-dishes of HEK239T cells (~ 1×10^7 cells per dish) were each transfected with 24 μg of FLAG-TRIM23. 48 h later, cells were lysed with Triton X-100 buffer (150 mM NaCl, 5% EDTA, 1% [v/v] Triton X-100, 50 mM HEPES pH 7.4, protease inhibitor cocktail [Sigma], and phosphatase inhibitor cocktail [Sigma]), followed by centrifugation at 13,000 rpm for 20 min at 4 °C. Post-centrifuged lysates were pre-cleared using 100 μl Sepharose® 4B (Sigma) to remove cell debris. A ~50% slurry of α-FLAG M2 Affinity Gel (Sigma) was added to lysates and incubated for 4 h at 4 °C, and beads were subsequently washed extensively with lysis buffer. Purified proteins were eluted in 2× Laemmli SDS sample buffer and heated for 5 min at 95 °C. Eluted proteins were separated on a NuPAGE 4–12% Bis-Tris gradient gel (Life Technologies). To stain the proteins on the gel, Coomassie Brilliant Blue (NuSep, Coomassie Electrophoresis Stain) was used. Bands corresponding to unmodified and ubiquitin-modified FLAG-TRIM23 were excised and analyzed by ion-trap mass spectrometry for posttranslational modifications at the Harvard Taplin Biological Mass Spectrometry Facility, Boston.

Viral Growth Assays

TRIM23 $^{+/+}$ and *TRIM23* $^{-/-}$ MEF cells, grown in 6-well plates, were infected with WT HSV-1 or mutHSV-1 at the indicated MOIs. Six hours later, supernatants were removed and cells were washed three times with PBS, followed by adding complete DMEM growth medium. 48 h later, supernatants were collected, and cell debris pelleted by centrifugation at 4,000 rpm for 10 min at 4 °C. Cleared supernatants from infected cells were serially diluted (10^1 – 10^8) in DMEM without supplements. Vero cells, grown in 96-well plates, were infected with diluted supernatants in 6 replicates per dilution. Cells were incubated 7–9 days, and an endpoint titer was calculated as a tissue culture infective dose 50% (TCID50) according to the Reed-Muench method[56].

For determining SINV replication in *TRIM23* $^{+/+}$ and *TRIM23* $^{-/-}$ MEF cells, ~ 3×10^5 cells were incubated in suspension with SINV (MOI 0.1 or 1) in DMEM supplemented with 5% FBS for 1 h. Next, cells were pelleted by centrifugation, washed twice with PBS, and seeded into 24-well plates containing complete DMEM. Eight hours later, virus-containing cell supernatants were collected and subjected to standard plaque assay. Briefly, BHK-21 cells, grown to confluency in 12-well plates, were infected for 1 h with 100 μL of serial dilutions of the virus-containing supernatants (in Dulbecco's Phosphate-Buffered Saline, Life Technologies, containing 1% FBS) mixed with 250 μL DMEM. Overlay medium containing 0.75% agarose (IBI Scientific, IB70051) in DMEM complemented with 5% FBS was added to cells, and cells incubated for 24 h until formation of plaques was visible. The agarose overlay was removed and cells were fixed in 4% (v/v) PFA in PBS (Santa Cruz) and stained with crystal violet (in 30% ethanol) to visualize plaques. Plaques were counted and

the infectious titer determined using the following equation: Virus titer (pfu/mL) = number of plaques × (1 mL / 0.1 mL) / fold of dilution.

For determining Ad-GFP replication, *TRIM23* $^{+/+}$ and *TRIM23* $^{-/-}$ MEF cells were grown in 24-well plates (~2 × 10^5 cells per well), and the next day infected with Ad-GFP at the indicated MOIs. Six hours later, cells were washed twice with PBS, followed by adding complete DMEM growth medium to cells. Cells were harvested 24 h later by detaching them using Trypsin-EDTA (Invitrogen), and then fixed in 2% (w/v) PFA (Santa Cruz) for 20 min. The percentage of GFP-positive cells was determined by FACS analysis using a BD LSRII 3–8 flow cytometer.

Colorimetric GTPase Assay

Five 10cm-dishes of HEK293T cells (~ 1×10^7 cells per dish) were each transfected with 20 μg of FLAG-TRIM23 WT or the indicated mutants. 48 h later, cells were lysed in Triton X-100 lysis buffer (150 mM NaCl, 5 mM EDTA, 1% [v/v] Triton X-100, 50 mM HEPES pH 7.4, and protease inhibitor cocktail [Sigma]), and cell debris pelleted by centrifugation at 13,000 rpm for 20 min at 4 °C. Cleared lysates were incubated with a ~50% slurry of FLAG M2 Agarose (Sigma) for 4 h at 4 °C. Precipitates were washed extensively with Triton X-100 buffer containing 500 mM NaCl, and immunoprecipitated proteins were eluted from the beads by incubation in 0.1 M sodium citrate (pH 2.5) for 15 min at 50 °C. Eluted samples were immediately neutralized with 1 M HEPES (pH 8.0). GTPase assay was performed using the ATPase/GTPase Activity Assay Kit (Sigma) according to the manufacturer's instructions. Briefly, eluted proteins were normalized using a Bicinchoninic acid (BCA) assay (Thermo Fisher Scientific) and incubated in the presence of GTP for 120 min at room temperature. After addition of the detection reagent, absorbance of samples was analyzed at 620 nm using a Molecular Devices VersaMax plate reader. Free phosphate values were calculated using a standard curve.

Luciferase-based GTPase Assay

Five 10cm-dishes of HEK293T cells (~ 1 × 10^7 cells per dish) were each transfected with 20 μg of FLAG-TRIM23 WT or the indicated mutants. 48 h later, cells were lysed in Triton X-100 buffer (150 mM NaCl, 5 mM EDTA, 1% [v/v] Triton X-100, 50 mM HEPES pH 7.4, and protease inhibitor cocktail [Sigma]), and cell debris pelleted by centrifugation at 13,000 rpm for 20 min at 4 °C. Cleared lysates were incubated with a ~50% slurry of FLAG M2 Agarose beads (Sigma) for 4 h at 4 °C. Beads were washed 3 times with Triton X-100 buffer containing 500 mM NaCl, and then twice with GTPase assay buffer (20 mM Tris pH 8.0, 10 mM DTT, 2.5 mM EDTA, 0.3 mg/mL BSA (Bovine Serum Albumin), 0.1 mg/mL cardiolipin [C0563, Sigma], and protease inhibitor cocktail [Sigma]). GTPase activity of the purified proteins was measured using the GTPase-Glo Kit (Promega) according to the manufacturer's instructions. Briefly, the purified proteins were incubated for 14 h at room temperature in GTPase-Glo-GEF (Guanine Exchange factor) buffer containing 10 μM GTP and 1 mM DTT. Next, the reconstituted GTPase-Glo buffer (GTPase Glo reagent 1:500, 10 mM ADP in GTPase-Glo buffer) was added to the samples and incubated for 30 min at room temperature. Ten minutes after addition of the Detection Reagent, luciferase luminescence was measured using a BioTek Synergy HT. GTPase activity values were

normalized to purified protein amounts, determined by BCA assay (Thermo Fisher Scientific), to account for differences in purification efficiency of TRIM23 WT and mutant proteins.

Alignments and Phylogenetic Tree

Primary sequence pairwise alignments were performed using Clustal Omega. The phylogenetic tree was generated by Clustal Omega as a neighbor-joining tree without distance corrections.

Homology Modeling

Homology models of the TRIM23 ARF domain (residues 402–574) were calculated using the automated subroutines of SWISS-MODEL at https://swissmodel.expasy.org[57]. From the available templates, ARF6 was selected due to its 55.5% sequence identity to the ARF domain of TRIM23, and because both GTP- and GDP-bound structures are available for ARF6 (PDB codes 2A5D and 1E0S, respectively)[58,59]. The GTP-bound forms of different ARF proteins adopt highly similar structures, whereas GDP-bound forms are more divergent. We therefore consider the GTP-bound model of the TRIM23 ARF domain to be more reliable.

Statistical analysis

To calculate P values for the TRIM siRNA screen, a two-way ANOVA assay was employed in R. Approximately 90 cells (3 × 30 cells) were quantified per sample. A P value of <0.05 was considered statistically significant.

For all other experiments, unpaired two-tailed Student's *t*-tests were used to compare differences between two unpaired experimental groups in all cases. A P value of <0.1 was considered statistically significant.

Data availability

The data that support the findings of this study are available from the corresponding author upon request. Complete western blot images of all figures in the manuscript are provided in Supplementary Figure 9.

Supplementary Material

Refer to Web version on PubMed Central for supplementary material.

Acknowledgments

We are grateful to A. García-Sastre (Icahn School of Medicine at Mount Sinai) and J. Jung (University of Southern California) for the TRIM cDNA library, and to S. Rabkin (Harvard) for providing mutant HSV-1. We also thank M. Ericsson (Harvard Electron Microscopy Facility) for assistance with sample preparation and S. Hwang (The University of Chicago) for helpful discussion. This study was supported in part by the US National Institutes of Health grant R01 AI087846 and R21 AI118509 (to M.U.G.) and R01 GM112508 (to O.P.). K.M.J.S. and F.F. were supported by fellowships from the German Research Foundation (SP 1600/1-1 and FU 949/1-1, respectively). G.P.R., J.K., J.M. and M.V. were supported by the Intramural Research Program of the NIH (National Heart, Lung, and Blood Institute). M.A.Z. received support by NIH training grant T32 GM007183.

References

1. Ozato K, Shin DM, Chang TH, Morse HC 3rd. TRIM family proteins and their emerging roles in innate immunity. Nature reviews. Immunology. 2008; 8:849–860. DOI: 10.1038/nri2413
2. Versteeg GA, et al. The E3-ligase TRIM family of proteins regulates signaling pathways triggered by innate immune pattern-recognition receptors. Immunity. 2013; 38:384–398. DOI: 10.1016/j.immuni.2012.11.013 [PubMed: 23438823]
3. Levine B, Kroemer G. Autophagy in the pathogenesis of disease. Cell. 2008; 132:27–42. DOI: 10.1016/j.cell.2007.12.018 [PubMed: 18191218]
4. Stolz A, Ernst A, Dikic I. Cargo recognition and trafficking in selective autophagy. Nature cell biology. 2014; 16:495–501. DOI: 10.1038/ncb2979 [PubMed: 24875736]
5. Randow F, Youle RJ. Self and nonself: how autophagy targets mitochondria and bacteria. Cell host & microbe. 2014; 15:403–411. DOI: 10.1016/j.chom.2014.03.012 [PubMed: 24721569]
6. Tal MC, Iwasaki A. Autophagy and innate recognition systems. Current topics in microbiology and immunology. 2009; 335:107–121. DOI: 10.1007/978-3-642-00302-8_5 [PubMed: 19802562]
7. Levine B, Mizushima N, Virgin HW. Autophagy in immunity and inflammation. Nature. 2011; 469:323–335. DOI: 10.1038/nature09782 [PubMed: 21248839]
8. Deretic V, Saitoh T, Akira S. Autophagy in infection, inflammation and immunity. Nature reviews. Immunology. 2013; 13:722–737. DOI: 10.1038/nri3532
9. Sharma S, et al. Triggering the interferon antiviral response through an IKK-related pathway. Science (New York, N.Y.). 2003; 300:1148–1151. DOI: 10.1126/science.1081315
10. Pilli M, et al. TBK-1 promotes autophagy-mediated antimicrobial defense by controlling autophagosome maturation. Immunity. 2012; 37:223–234. DOI: 10.1016/j.immuni.2012.04.015 [PubMed: 22921120]
11. Richter B, et al. Phosphorylation of OPTN by TBK1 enhances its binding to Ub chains and promotes selective autophagy of damaged mitochondria. Proceedings of the National Academy of Sciences of the United States of America. 2016; 113:4039–4044. DOI: 10.1073/pnas.1523926113 [PubMed: 27035970]
12. Lei Y, et al. The mitochondrial proteins NLRX1 and TUFM form a complex that regulates type I interferon and autophagy. Immunity. 2012; 36:933–946. DOI: 10.1016/j.immuni.2012.03.025 [PubMed: 22749352]
13. Allen IC, et al. NLRX1 protein attenuates inflammatory responses to infection by interfering with the RIG-I-MAVS and TRAF6-NF-kappaB signaling pathways. Immunity. 2011; 34:854–865. DOI: 10.1016/j.immuni.2011.03.026 [PubMed: 21703540]
14. Mandell MA, et al. TRIM proteins regulate autophagy and can target autophagic substrates by direct recognition. Developmental cell. 2014; 30:394–409. DOI: 10.1016/j.devcel.2014.06.013 [PubMed: 25127057]
15. Orvedahl A, et al. HSV-1 ICP34.5 confers neurovirulence by targeting the Beclin 1 autophagy protein. Cell host & microbe. 2007; 1:23–35. DOI: 10.1016/j.chom.2006.12.001 [PubMed: 18005679]
16. Kanai R, et al. Effect of gamma34.5 deletions on oncolytic herpes simplex virus activity in brain tumors. Journal of virology. 2012; 86:4420–4431. DOI: 10.1128/JVI.00017-12 [PubMed: 22345479]
17. Kuma A, et al. The role of autophagy during the early neonatal starvation period. Nature. 2004; 432:1032–1036. DOI: 10.1038/nature03029 [PubMed: 15525940]
18. Meza-Carmen V, et al. Regulation of growth factor receptor degradation by ADP-ribosylation factor domain protein (ARD) 1. Proceedings of the National Academy of Sciences of the United States of America. 2011; 108:10454–10459. DOI: 10.1073/pnas.1103867108 [PubMed: 21653881]
19. Bjorkoy G, et al. p62/SQSTM1 forms protein aggregates degraded by autophagy and has a protective effect on huntingtin-induced cell death. The Journal of cell biology. 2005; 171:603–614. DOI: 10.1083/jcb.200507002 [PubMed: 16286508]

20. Pankiv S, et al. p62/SQSTM1 binds directly to Atg8/LC3 to facilitate degradation of ubiquitinated protein aggregates by autophagy. The Journal of biological chemistry. 2007; 282:24131–24145. DOI: 10.1074/jbc.M702824200 [PubMed: 17580304]
21. Arimoto K, et al. Polyubiquitin conjugation to NEMO by triparite motif protein 23 (TRIM23) is critical in antiviral defense. Proceedings of the National Academy of Sciences of the United States of America. 2010; 107:15856–15861. doi:1004621107 [pii]. DOI: 10.1073/pnas.1004621107 [PubMed: 20724660]
22. Laurent-Rolle M, et al. The interferon signaling antagonist function of yellow fever virus NS5 protein is activated by type I interferon. Cell host & microbe. 2014; 16:314–327. DOI: 10.1016/j.chom.2014.07.015 [PubMed: 25211074]
23. Orvedahl A, et al. Autophagy protects against Sindbis virus infection of the central nervous system. Cell host & microbe. 2010; 7:115–127. DOI: 10.1016/j.chom.2010.01.007 [PubMed: 20159618]
24. Montespan C, et al. Multi-layered control of Galectin-8 mediated autophagy during adenovirus cell entry through a conserved PPxY motif in the viral capsid. PLoS pathogens. 2017; 13:e1006217. [PubMed: 28192531]
25. Vitale N, Moss J, Vaughan M. ARD1, a 64-kDa bifunctional protein containing an 18-kDa GTP-binding ADP-ribosylation factor domain and a 46-kDa GTPase-activating domain. Proceedings of the National Academy of Sciences of the United States of America. 1996; 93:1941–1944. [PubMed: 8700863]
26. Vichi A, Payne DM, Pacheco-Rodriguez G, Moss J, Vaughan M. E3 ubiquitin ligase activity of the trifunctional ARD1 (ADP-ribosylation factor domain protein 1). Proceedings of the National Academy of Sciences of the United States of America. 2005; 102:1945–1950. DOI: 10.1073/pnas.0409800102 [PubMed: 15684077]
27. Mevissen TE, et al. OTU deubiquitinases reveal mechanisms of linkage specificity and enable ubiquitin chain restriction analysis. Cell. 2013; 154:169–184. DOI: 10.1016/j.cell.2013.05.046 [PubMed: 23827681]
28. Cherfils J. Arf GTPases and their effectors: assembling multivalent membrane-binding platforms. Current opinion in structural biology. 2014; 29:67–76. DOI: 10.1016/j.sbi.2014.09.007 [PubMed: 25460270]
29. D'Souza-Schorey C, Chavrier P. ARF proteins: roles in membrane traffic and beyond. Nature reviews. Molecular cell biology. 2006; 7:347–358. DOI: 10.1038/nrm1910 [PubMed: 16633337]
30. Vitale N, Horiba K, Ferrans VJ, Moss J, Vaughan M. Localization of ADP-ribosylation factor domain protein 1 (ARD1) in lysosomes and Golgi apparatus. Proceedings of the National Academy of Sciences of the United States of America. 1998; 95:8613–8618. [PubMed: 9671726]
31. Kuma A, Mizushima N, Ishihara N, Ohsumi Y. Formation of the approximately 350-kDa Apg12-Apg5.Apg16 multimeric complex, mediated by Apg16 oligomerization, is essential for autophagy in yeast. The Journal of biological chemistry. 2002; 277:18619–18625. DOI: 10.1074/jbc.M111889200 [PubMed: 11897782]
32. Thurston TL, et al. Recruitment of TBK1 to cytosol-invading Salmonella induces WIPI2-dependent antibacterial autophagy. The EMBO journal. 2016; 35:1779–1792. DOI: 10.15252/embj.201694491 [PubMed: 27370208]
33. Clark K, Plater L, Peggie M, Cohen P. Use of the pharmacological inhibitor BX795 to study the regulation and physiological roles of TBK1 and IkappaB kinase epsilon: a distinct upstream kinase mediates Ser-172 phosphorylation and activation. The Journal of biological chemistry. 2009; 284:14136–14146. DOI: 10.1074/jbc.M109.000414 [PubMed: 19307177]
34. Matsumoto G, Wada K, Okuno M, Kurosawa M, Nukina N. Serine 403 phosphorylation of p62/SQSTM1 regulates selective autophagic clearance of ubiquitinated proteins. Molecular cell. 2011; 44:279–289. DOI: 10.1016/j.molcel.2011.07.039 [PubMed: 22017874]
35. Soulat D, et al. The DEAD-box helicase DDX3X is a critical component of the TANK-binding kinase 1-dependent innate immune response. The EMBO journal. 2008; 27:2135–2146. DOI: 10.1038/emboj.2008.126 [PubMed: 18583960]
36. Larabi A, et al. Crystal structure and mechanism of activation of TANK-binding kinase 1. Cell reports. 2013; 3:734–746. DOI: 10.1016/j.celrep.2013.01.034 [PubMed: 23453971]

37. Tu D, et al. Structure and ubiquitination-dependent activation of TANK-binding kinase 1. Cell reports. 2013; 3:747–758. DOI: 10.1016/j.celrep.2013.01.033 [PubMed: 23453972]
38. Ma X, et al. Molecular basis of Tank-binding kinase 1 activation by transautophosphorylation. Proceedings of the National Academy of Sciences of the United States of America. 2012; 109:9378–9383. DOI: 10.1073/pnas.1121552109 [PubMed: 22619329]
39. Kimura T, et al. TRIM-mediated precision autophagy targets cytoplasmic regulators of innate immunity. The Journal of cell biology. 2015; 210:973–989. DOI: 10.1083/jcb.201503023 [PubMed: 26347139]
40. Kimura T, et al. Dedicated SNAREs and specialized TRIM cargo receptors mediate secretory autophagy. The EMBO journal. 2017; 36:42–60. DOI: 10.15252/embj.201695081 [PubMed: 27932448]
41. Tsuchida T, et al. The ubiquitin ligase TRIM56 regulates innate immune responses to intracellular double-stranded DNA. Immunity. 2010; 33:765–776. DOI: 10.1016/j.immuni.2010.10.013 [PubMed: 21074459]
42. Gack MU, et al. TRIM25 RING-finger E3 ubiquitin ligase is essential for RIG-I-mediated antiviral activity. Nature. 2007; 446:916–920. [PubMed: 17392790]
43. Narayan K, et al. TRIM13 is a negative regulator of MDA5-mediated type I interferon production. Journal of virology. 2014; 88:10748–10757. DOI: 10.1128/JVI.02593-13 [PubMed: 25008915]
44. Matsumoto G, Shimogori T, Hattori N, Nukina N. TBK1 controls autophagosomal engulfment of polyubiquitinated mitochondria through p62/SQSTM1 phosphorylation. Human molecular genetics. 2015; 24:4429–4442. DOI: 10.1093/hmg/ddv179 [PubMed: 25972374]
45. Zaffagnini G, Martens S. Mechanisms of Selective Autophagy. Journal of molecular biology. 2016; 428:1714–1724. DOI: 10.1016/j.jmb.2016.02.004 [PubMed: 26876603]
46. Li S, Wang L, Berman M, Kong YY, Dorf ME. Mapping a dynamic innate immunity protein interaction network regulating type I interferon production. Immunity. 2011; 35:426–440. DOI: 10.1016/j.immuni.2011.06.014 [PubMed: 21903422]
47. Davis ME, Gack MU. Ubiquitination in the antiviral immune response. Virology. 2015; 479–480c: 52–65. DOI: 10.1016/j.virol.2015.02.033
48. Ni HM, et al. Dissecting the dynamic turnover of GFP-LC3 in the autolysosome. Autophagy. 2011; 7:188–204. [PubMed: 21107021]
49. Ding WX, et al. Linking of autophagy to ubiquitin-proteasome system is important for the regulation of endoplasmic reticulum stress and cell viability. The American journal of pathology. 2007; 171:513–524. DOI: 10.2353/ajpath.2007.070188 [PubMed: 17620365]
50. Feng Y, Longmore GD. The LIM protein Ajuba influences interleukin-1-induced NF-kappaB activation by affecting the assembly and activity of the protein kinase Czeta/p62/TRAF6 signaling complex. Molecular and cellular biology. 2005; 25:4010–4022. DOI: 10.1128/mcb.25.10.4010-4022.2005 [PubMed: 15870274]
51. Liang C, et al. Autophagic and tumour suppressor activity of a novel Beclin1-binding protein UVRAG. Nature cell biology. 2006; 8:688–699. DOI: 10.1038/ncb1426 [PubMed: 16799551]
52. Wang L, Li S, Dorf ME. NEMO binds ubiquitinated TANK-binding kinase 1 (TBK1) to regulate innate immune responses to RNA viruses. PloS one. 2012; 7:e43756. [PubMed: 23028469]
53. Lim KL, et al. Parkin mediates nonclassical, proteasomal-independent ubiquitination of synphilin-1: implications for Lewy body formation. J Neurosci. 2005; 25:2002–2009. DOI: 10.1523/JNEUROSCI.4474-04.2005 [PubMed: 15728840]
54. Livingston CM, Ifrim MF, Cowan AE, Weller SK. Virus-Induced Chaperone-Enriched (VICE) domains function as nuclear protein quality control centers during HSV-1 infection. PLoS pathogens. 2009; 5:e1000619. [PubMed: 19816571]
55. Kimura S, Noda T, Yoshimori T. Dissection of the autophagosome maturation process by a novel reporter protein, tandem fluorescent-tagged LC3. Autophagy. 2007; 3:452–460. [PubMed: 17534139]
56. Gaush CR, Youngner JS. A tissue culture color test for measuring influenza virus and antibody. Proceedings of the Society for Experimental Biology and Medicine. Society for Experimental Biology and Medicine. 1959; 101:853–856.

57. Biasini M, et al. SWISS-MODEL: modelling protein tertiary and quaternary structure using evolutionary information. Nucleic Acids Res. 2014; 42:W252–258. DOI: 10.1093/nar/gku340 [PubMed: 24782522]

58. O'Neal CJ, Jobling MG, Holmes RK, Hol WG. Structural basis for the activation of cholera toxin by human ARF6-GTP. Science (New York, N.Y.). 2005; 309:1093–1096. DOI: 10.1126/science.1113398

59. Menetrey J, Macia E, Pasqualato S, Franco M, Cherfils J. Structure of Arf6-GDP suggests a basis for guanine nucleotide exchange factors specificity. Nat Struct Biol. 2000; 7:466–469. DOI: 10.1038/75863 [PubMed: 10881192]

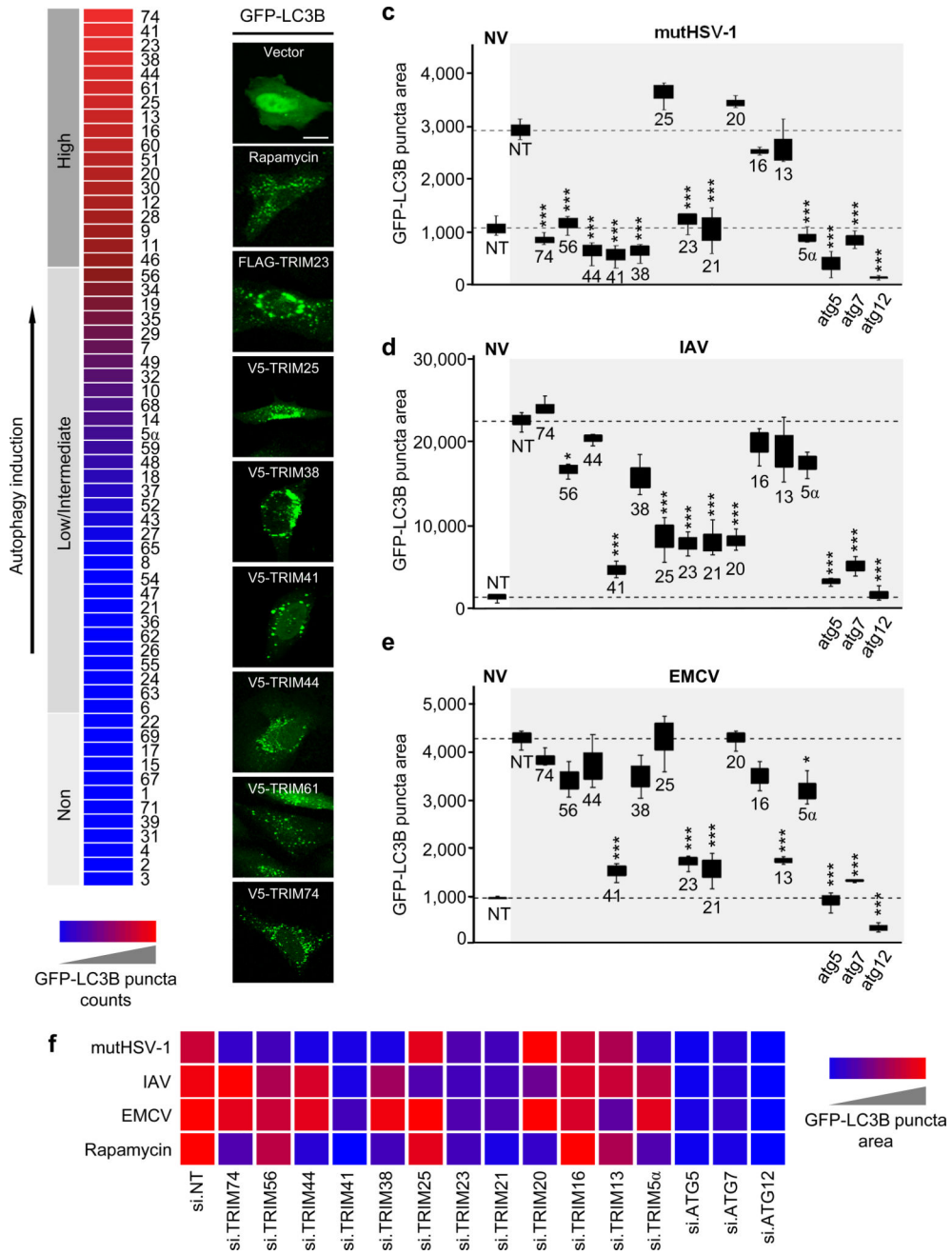

Figure 1. TRIM proteins modulate viral-induced autophagy in a virus species-specific manner

a, Summary of the TRIM cDNA screen (shown in Supplementary Fig. 1a) in which 61 TRIM proteins were tested for their ability to induce GFP-LC3B puncta formation in transiently transfected HeLa cells. TRIM proteins were categorized into ‘high inducers’ of autophagy (red; defined as inducing more GFP-LC3B puncta than rapamycin stimulation), or ‘low/intermediate inducers’ and ‘non-inducers’ (magenta/blue; defined as inducing fewer GFP-LC3B puncta than rapamycin but more than empty vector transfection, or similar to vector transfection, respectively). **b,** Representative laser-scanning confocal microscopy images of GFP-LC3B puncta formation in HeLa cells for the top 7 hits from the TRIM

cDNA screen shown in (a). Representative images for GFP-LC3B puncta formation induced by rapamycin treatment or empty vector transfection (controls) are also shown. Scale bar, 20 μm. **c–e,** GFP-LC3B puncta formation in HeLa cells transiently transfected with non-targeting control siRNA (NT) or siRNAs targeting the indicated TRIM proteins and subsequently infected with mutHSV-1 (MOI 4) for 8 h (c), IAV (MOI 5) for 14 h (d), or EMCV (MOI 100) for 6 h (e). Box and whisker plots show the distribution of the area of GFP-LC3B for 3 individual images, each containing ~30 cells. **f,** Summary of the results of GFP-LC3B puncta formation from the RNAi screen using viral stimuli (c-e) or rapamycin treatment (Supplementary Fig. 1d). NV, no infection. *$p<0.05$, ***$p<0.0005$ (ANOVA test). Data are representative of one screen (**a**), or two (**b**) or three (**c–f**) independent experiments.

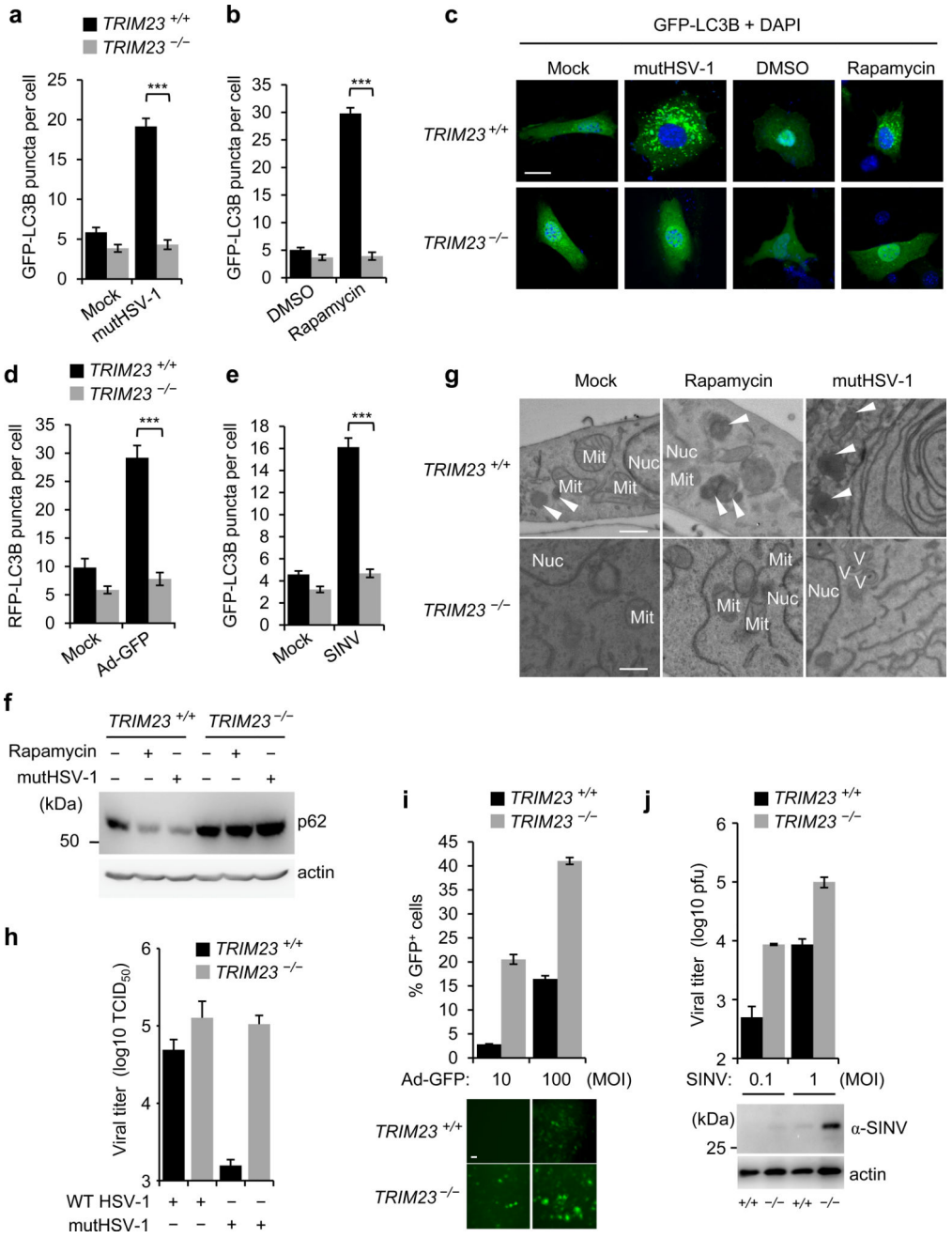

Figure 2. TRIM23 is essential for virus-induced autophagy

a,b, GFP-LC3B puncta formation in *TRIM23* $^{+/+}$ or *TRIM23* $^{-/-}$ MEFs transiently transfected with GFP-LC3B and either left uninfected (Mock) or infected with mutHSV-1 (MOI 4) for 12 h, or treated with DMSO or rapamycin for 2 h. Results represent the mean GFP-LC3B puncta per cell ± SD (n=50). ***p<0.001 (Student's *t*-test). **c,** Representative images of GFP-LC3B puncta formation for the experiments shown in (a,b). Scale bar, 20 μm. **d,e,** Quantification of RFP-LC3B or GFP-LC3B puncta in transiently transfected *TRIM23* $^{+/+}$ or *TRIM23* $^{-/-}$ MEFs that were left uninfected (Mock), or infected with Ad-GFP (MOI 100) for 48 h or SINV (MOI 5) for 24 h. Results represent the mean RFP/GFP-

LC3B puncta per cell ± SD (n=50). ***p<0.001 (Student's *t*-test). **f,** Endogenous p62 protein levels in the whole cell lysates (WCLs) of *TRIM23* $^{+/+}$ and *TRIM23* $^{-/-}$ MEFs that were either left uninfected, infected with mutHSV-1 (MOI 4) for 12 h, or stimulated with rapamycin for 2 h, determined by immunoblot (IB) with anti-p62. **g,** EM analysis of *TRIM23* $^{+/+}$ and *TRIM23* $^{-/-}$ MEFs that were mock-treated, stimulated with rapamycin for 2 h, or infected with mutHSV-1 (MOI 4) for 12 h. Arrows indicate autophagolysosomes. Nuc, nucleus; Mit, mitochondrion; V, virus particle. Scale bar, 500 nm. **h,** Replication of WT HSV-1 and mutHSV-1 (both MOI 0.1) in *TRIM23* $^{+/+}$ and *TRIM23* $^{-/-}$ MEFs, determined by $TCID_{50}$ assay at 48 hours postinfection (h.p.i.). Results are expressed as mean ± SD (n=2). **i,** Replication of Ad-GFP (MOI 10 and 100) in *TRIM23* $^{+/+}$ and *TRIM23* $^{-/-}$ MEFs, determined by analyzing GFP-positive cells using FACS (upper panel) or microscopy (lower panel) at 24 h.p.i. Results are expressed as mean ±SD (n=3). Scale bar, 20 μm. **j,** Replication of SINV (MOI 0.1 and 1) in *TRIM23* $^{+/+}$ and *TRIM23* $^{-/-}$ MEFs, determined by plaque assay (upper panel), or IB of WCLs using anti-SINV antibody (lower panel) at 16 h.p.i. Results are expressed as mean ± SD (n=3). Data are representative of at least two independent experiments (**a–f,h–j**), or one representative image from multiple datasets (**g**).

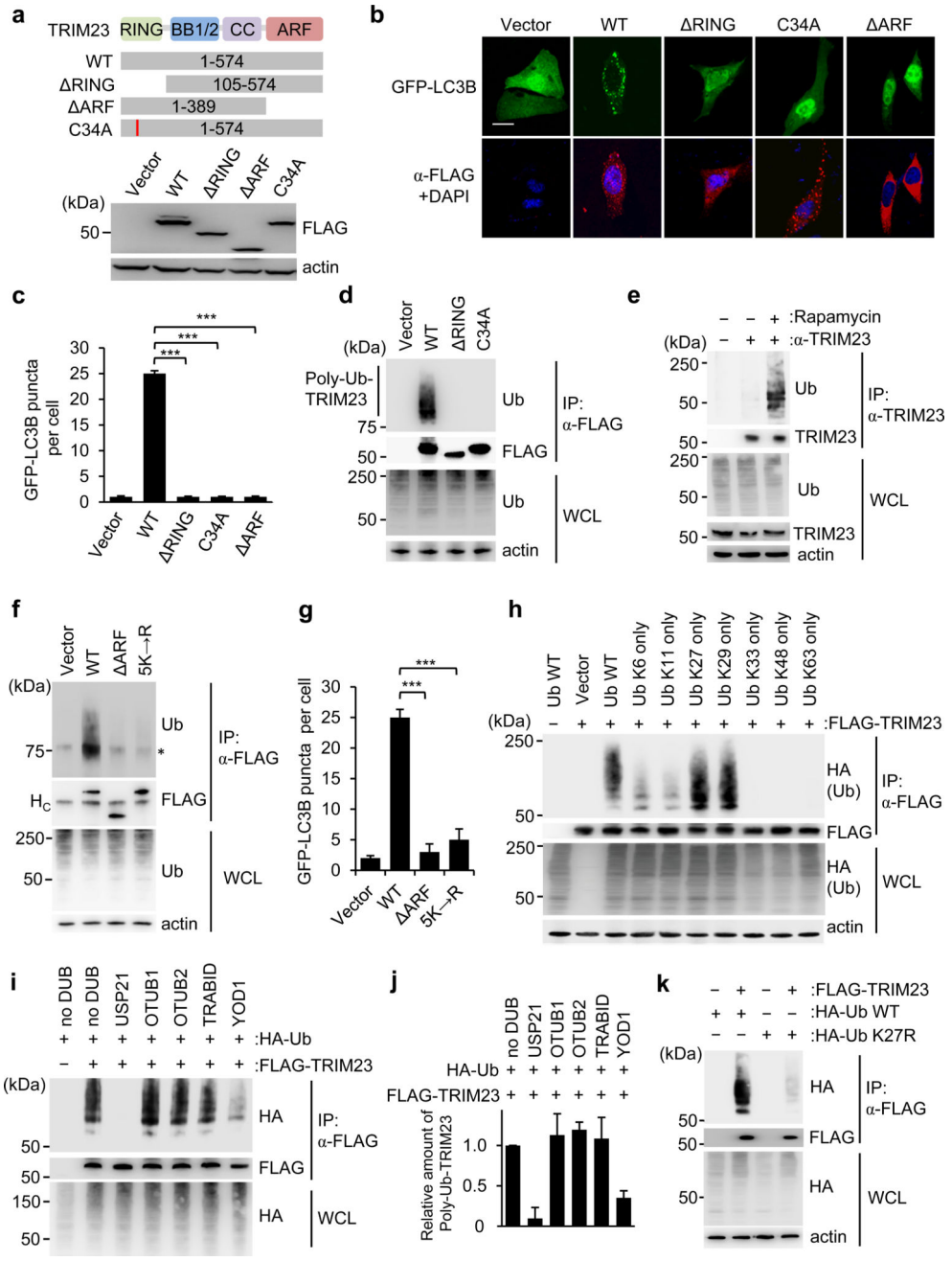

Figure 3. K27-linked auto-ubiquitination of the ARF domain of TRIM23 is necessary for its autophagy function

a, TRIM23 domain structure and mutant constructs. Numbers indicate amino acids. Efficient expression of TRIM23 WT and mutants was confirmed in transiently transfected HEK293T cells by IB with anti-FLAG. RING, Really Interesting New Gene domain; BB1/2, B-Box 1 and 2; CC, coiled-coil; ARF, ADP-ribosylation factor domain. **b,** GFP-LC3B puncta formation in *TRIM23* $^{-/-}$ MEFs transiently transfected with GFP-LC3B (green) and either empty vector, or the indicated FLAG-tagged TRIM23 constructs (red). DAPI, nuclei (blue). Scale bar, 20 μm. **c,** Quantification of GFP-LC3B puncta for (b). Results represent the mean

GFP-LC3B puncta per cell ± SD (n=50). ***p <0.001 (Student's *t*-test). **d,** Ubiquitination of FLAG-TRIM23 WT and mutants in transiently transfected HEK293T cells, determined by immunoprecipitation (IP) with anti-FLAG and IB with anti-ubiquitin (Ub) at 48 h post-transfection. **e,** Ubiquitination of endogenous TRIM23 in HEK293T cells that were either mock-treated or stimulated with rapamycin for 4 h, determined by IP with anti-TRIM23 and IB with anti-Ub. **f,** Ubiquitination of FLAG-tagged TRIM23 WT and mutants in transiently transfected HEK293T cells, assessed by IP with anti-FLAG and IB with anti-Ub at 48 h post-transfection. Asterisk indicates unspecific band. H_C indicates antibody heavy chain. **g,** Quantification of GFP-LC3B puncta in GFP-LC3B-HeLa cells transiently transfected with empty vector or the indicated TRIM23 constructs (FLAG-tagged). Results represent the mean GFP-LC3B puncta per cell ± SD (n=30). **h,** Ubiquitination of FLAG-TRIM23 in transiently transfected HEK293T cells co-expressing HA-tagged WT ubiquitin (Ub WT) or the indicated Ub mutants, assessed by IP with anti-FLAG and IB with anti-HA at 48 h post-transfection. **i,** *In vitro* DUB restriction assay of FLAG-TRIM23 purified from transfected HEK293T cells co-expressing HA-Ub WT. TRIM23 protein was incubated with the indicated DUB enzymes, followed by IB with anti-HA. **j,** Polyubiquitination (poly-Ub) of TRIM23 from (i) was quantified by densitometry. Results represent the mean of two independent experiments ± SD. **k,** Ubiquitination of FLAG-TRIM23 in transiently transfected HEK293T cells that co-expressed either HA-tagged WT Ub, or the K27R Ub mutant. 48 h later, WCLs were subjected to IP with anti-FLAG, followed by IB with anti-HA. Data are representative of two (**a–c,e,i–k**) or three (**d,f,g,h**) independent experiments.

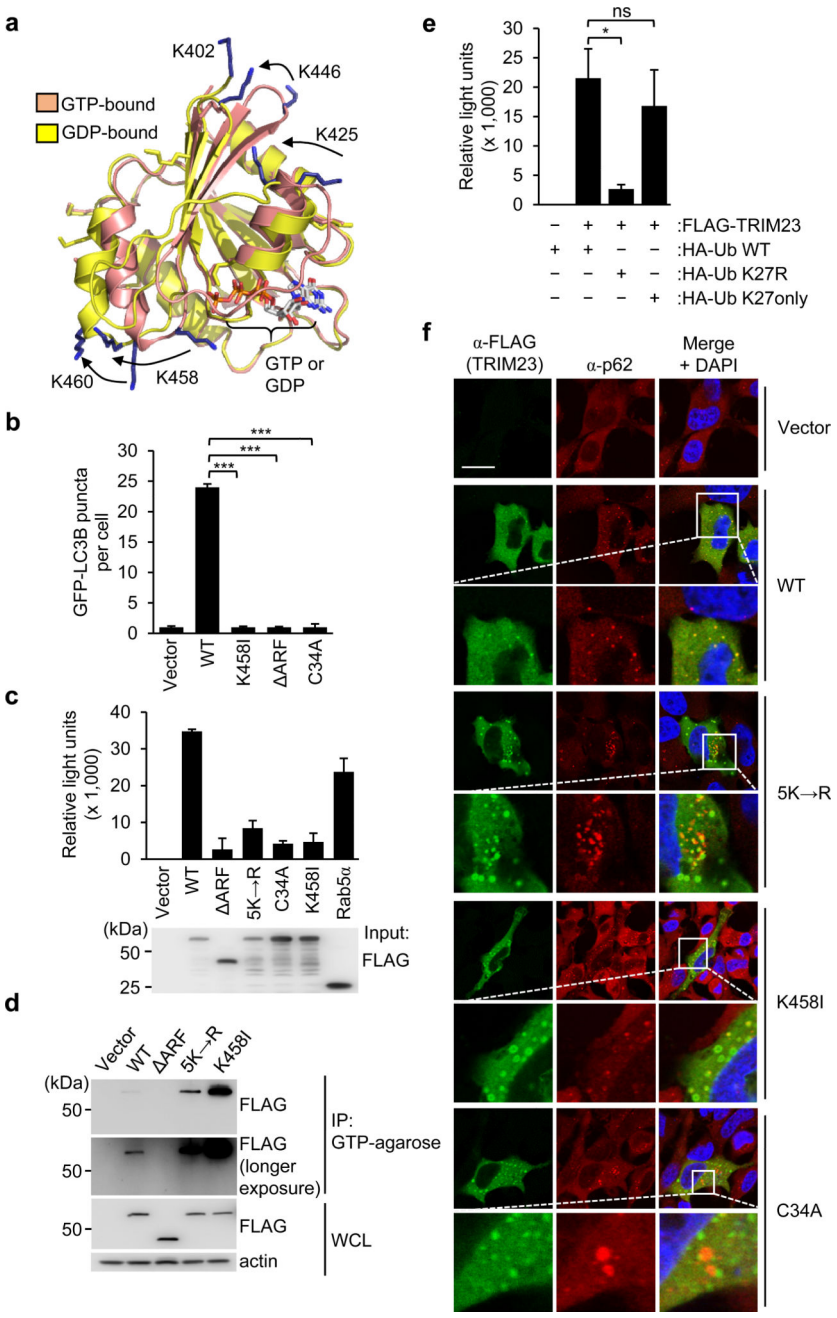

Figure 4. ARF ubiquitination is required for the GTP hydrolysis activity of TRIM23 and its localization to autophagosomes

a, Homology models of the TRIM23 ARF domain (residues 402–574) based upon the GTP- and GDP-bound forms of ARF6. The five lysines that comprise the main sites of auto-ubiquitination are shown as blue sticks, with positional differences indicated by arrows (GTP to GDP). The position of K402 is shown only for the GDP-bound form as this residue is absent from the GTP-bound homology model. The active site containing bound nucleotide is indicated on the lower right. **b,** Quantification of GFP-LC3B puncta in *TRIM23* $^{-/-}$ MEF cells transiently transfected with GFP-LC3B together with empty vector, or the indicated FLAG-tagged TRIM23 constructs. 48 h later, cells were stained with anti-FLAG antibody,

and GFP-LC3B puncta were quantified in cells positive for anti-FLAG-staining. Results represent the mean LC3B puncta per cell ± SD (n=30). ***p <0.001 (Student's *t*-test). **c,** *In vitro* GTPase activity of purified FLAG-tagged TRIM23 WT and mutants, or Rab5α (positive control). Purified proteins were incubated with GTP *in vitro*, followed by measuring GTP hydrolysis using a luciferase-based readout. Results are expressed as mean ± SD (n=3). **d,** Binding of TRIM23 WT and mutants to GTP-coupled agarose. FLAG-tagged TRIM23 constructs were expressed in transiently transfected HEK293T cells. 48 h later, WCLs were incubated with GTP-agarose and proteins bound to GTP determined by IB with anti-FLAG antibody. **e,** *In vitro* GTPase activity of purified FLAG-tagged TRIM23 WT from cells co-expressing HA-tagged Ub WT, or the Ub mutants K27R or K27only. Purified TRIM23 WT was incubated with GTP *in vitro,* followed by measuring GTP hydrolysis activity as described in (c). Results are expressed as mean ± SD (n=3). *p <0.1 (Student's *t*-test). ns, statistically not significant. **f,** Co-localization of endogenous p62 with FLAG-tagged TRIM23 WT or mutants in transiently transfected HeLa cells, determined by immunostaining with anti-FLAG (TRIM23, green) and anti-p62 (red), followed by confocal microscopy analysis. DAPI, nuclei (blue); Scale bar, 20 μm. Data are representative of one (**a**), or at least two (**b–f**) independent experiments.

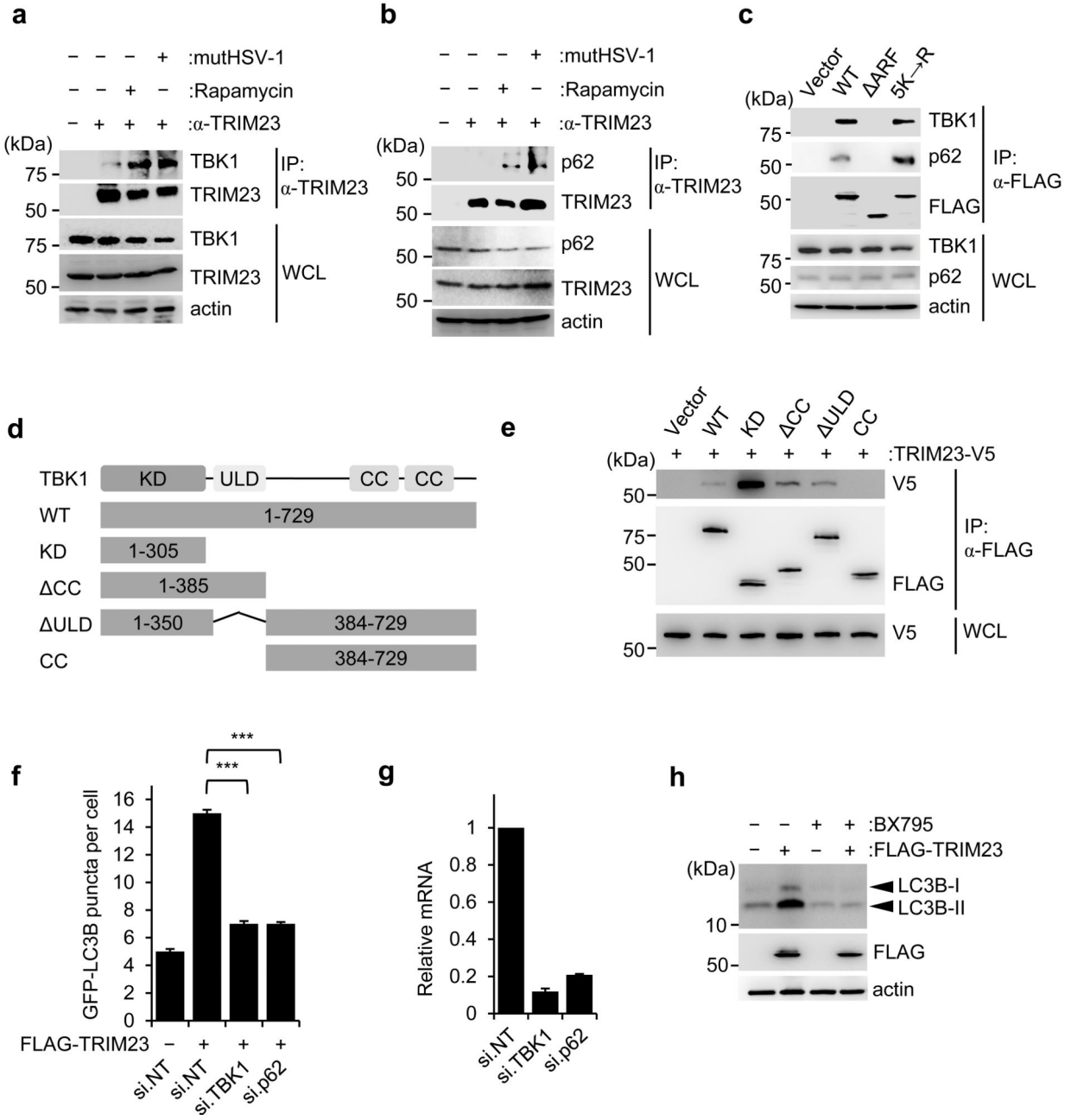

Figure 5. TRIM23 interacts with TBK1 and p62

a, Binding of endogenous TBK1 to TRIM23 in HEK293T cells that were mock-treated, infected with mutHSV-1 (MOI 4) for 12 h, or treated with rapamycin for 2 h, determined by IP with anti-TRIM23 and IB with anti-TBK1. **b,** Binding of endogenous p62 to TRIM23 in HEK293T cells stimulated as in (a), assessed by IP with anti-TRIM23 and IB with anti-p62. **c,** Binding of endogenous p62 and TBK1 to FLAG-tagged TRIM23 WT or its mutants in transiently transfected HEK293T cells, assessed by IP with anti-FLAG and IB with anti-TBK1 and anti-p62 at 48 h post-transfection. **d,** Schematic representation of TBK1 domain structure and mutant constructs used for mapping studies. Numbers indicate amino acids.

KD, kinase domain; ULD, ubiquitin-like domain; CC, coiled-coil domain. **e,** Binding of TRIM23-V5 to FLAG-tagged TBK1 WT or mutants in transiently transfected HEK293T cells, determined by IP with anti-FLAG and IB with anti-V5 at 48 h post-transfection. **f,** Quantification of GFP-LC3B puncta in HEK293T cells transiently transfected with GFP-LC3B together with empty vector or FLAG-TRIM23 and either non-targeting control siRNA (si.NT), or siRNAs targeting TBK1 or p62 (si.TBK1 or si.p62). Results represent the mean GFP-LC3B puncta per cell ± SD (n=30). ***p<0.001 (Student's *t*-test). **g,** Representative knockdown efficiency of endogenous TBK1 and p62 for the experiment shown in (f), determined by qRT-PCR. Results represent the mean ± SD (n=3). **h,** Endogenous LC3B-I-to-II conversion in HEK293T cells that were transiently transfected with empty vector or FLAG-TRIM23 for 48 h and subsequently mock-treated or treated with BX795 for 4 h, assessed by IB with anti-LC3B. Data are representative of at least two (**a–b,e–h**) or three (**c**) independent experiments.

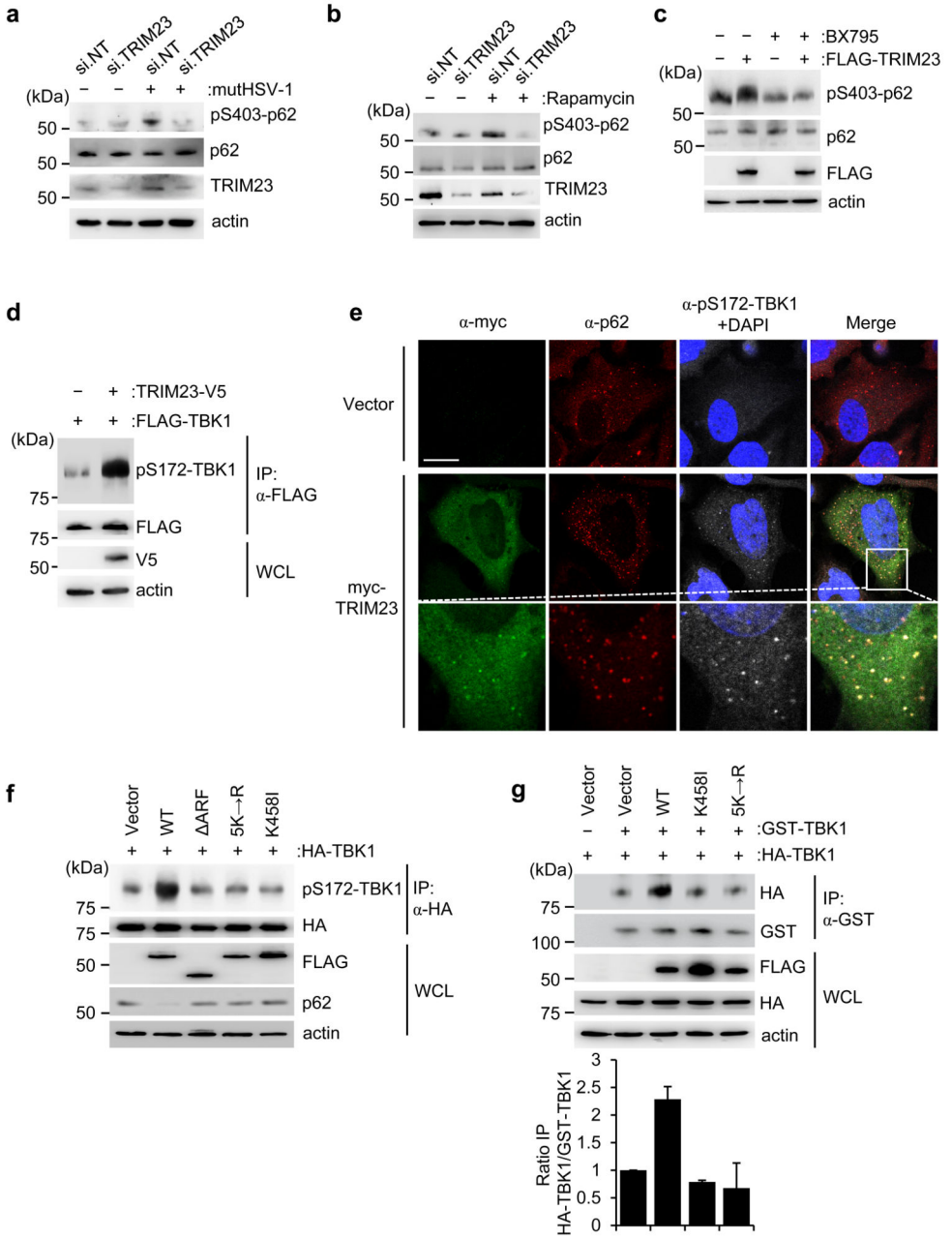

Figure 6. TRIM23 GTPase activates TBK1 to phosphorylate p62

a,b, Endogenous p62 phosphorylation at S403 in the WCLs of HEK293T cells that were transfected with si.NT or si.TRIM23 for 48 h and then either mock-treated, infected with mutHSV-1 (MOI 10) for 3 h (a), or treated with rapamycin for 4 h (b), determined by IB with anti-pS403-p62. Knockdown of endogenous TRIM23 was confirmed by IB with anti-TRIM23. **c,** Endogenous p62 phosphorylation at S403 in the WCLs of HEK293T cells that were transfected with empty vector or FLAG-TRIM23 for 44 h and then mock-treated or treated with BX795 for 4 h, determined by IB with anti-pS403-p62. **d,** S172 phosphorylation of FLAG-TBK1 in transiently transfected HEK293T cells that co-expressed empty vector or

TRIM23-V5, determined by IP with anti-FLAG, followed by IB with anti-pS172-TBK1. **e,** Laser scanning confocal microscopy analysis of the co-localization of transiently transfected myc-TRIM23 with endogenous phospho-(p)-S172-TBK1 and p62 in HeLa cells, determined by immunostaining with anti-myc (green), anti-pS172-TBK1 (grey), and anti-p62 (red) antibodies at 48 h post-transfection. DAPI, nuclei (blue). Scale bar, 20 μm. **f,** S172 phosphorylation of HA-TBK1 in HEK293T cells that were co-transfected with empty vector or FLAG-tagged TRIM23 WT or mutants, determined by IP with anti-HA and IB with anti-pS172-TBK1 at 48 h post-transfection. **g,** Upper panel: TBK1 dimerization assessed by co-purifying HA-TBK1 and GST-TBK1 in transiently transfected HEK293T cells that also co-expressed either empty vector, or FLAG-tagged TRIM23 WT or mutants, determined by IP with anti-GST and IB with anti-HA at 48 h post-transfection. Lower panel: Dimerization of GST-TBK1 and HA-TBK1 was quantified by densitometry, and data shown represent the mean of two independent experiments ± SD. Data are representative of at least two independent experiments (**a–g**).